THE UNIVERSITY OF ALBERTA

LOW-LEVEL ATMOSPHERIC STRUCTURE OVER CALGARY IN PRE-CHINOOK CONDITIONS

BY

© A. R. KELLIE

A THESIS

SUBMITTED TO THE FACULTY OF GRADUATE STUDIES AND RESEARCH

IN PARTIAL FULFILMENT OF THE REQUIREMENTS FOR THE DEGREE

OF MASTER OF SCIENCE

DEPARTMENT OF GEOGRAPHY

EDMONTON, ALBERTA

FALL, 1972

ABSTRACT

This study is concerned with the low-level structure of the atmosphere prior to and during Chinook-type surface warming.

The investigation was carried out using data collected on an instrumented 91 m tower in Calgary, Alberta. The tower was instrumented at four levels for measuring temperature and two levels for measuring wind. For this study periods with strong westerly flow aloft and statically-stable conditions to great heights were chosen from the winter months (November - March), 1970-1971.

It was found that there were abnormal fluctuations (typical magnitude 2-6C) in the temperatures at all four levels beginning as much as 18 hours ahead of the surface warming. The surface warming took the form of a rapid breakdown of the ground-based inversion.

The analysis consists of calculations of variance spectra and complex cross-spectra of the four levels of temperatures. Variance spectra of these fluctuations revealed that the periods that contributed most to the variance ranged from about 30 to 130 min. Short-period contributions to the variance were almost negligible compared with those of longer periods.

The cospectral calculations showed that the frequencies that contributed most to the covariance of temperature between levels were in the same range as those values calculated from the variance

spectra. Also, it was in this range of frequencies that statistically-significant coherences were found.

The spectral analysis was unable to resolve a consistent phase angle relationship between levels on the tower. It is suggested that either the levels on the tower are essentially oscillating in unison or that the phase angle was obscured by averaging involved in the calculations.

A calculation of the amplitudes at each level revealed two classes of events. The first was characterized by amplitudes that increased with height, and the second by amplitudes that remained more or less uniform with height.

An analysis of the vertical shear of the horizontal wind speed, vertical temperature gradient, and Richardson number was performed. Values of the shear were calculated to be as large as 10 m sec^{-1} $(100\ m)^{-1}$ prior to or during the inversion breakdown. Values of the Richardson number were found to be less than +0.25 prior to or during the inversion breakdown. For these reasons, a Kelvin-Helmholtz type of shearing instability is suggested and this instability is put forth as a possible source of low-level turbulence.

The large temperature oscillations appeared to be reproduced on a second tower 12 km upwind. Estimates of the wavelength based on data from both towers ranged from 29 to 118 km. However, because of timing uncertainties, the results are uncertain.

ACKNOWLEDGEMENTS

Without the assistance of a number of people and organizations this study would not have been possible.

In particular I would like to single out the contributions of a good friend and colleague, J. D. Steenbergen.

To Miss J. H. Dubbeldam who provided many hours of assistance in data gathering I am extremely grateful.

A staff member, not on my examining committee, Dr. E. P. Lozowski, was always available for discussion.

Throughout this study an invaluable convenience was the open library belonging to Professor R. W. Longley.

I would also like to thank my supervisor, Dr. K. D. Hage for suggesting the project and for his encouragement and advice.

The Institute of Earth and Planetary Physics kindly provided computing facilities in the form of a Nova 1200.

The able assistance of Mrs. Laura Smith who typed this manuscript is greatly appreciated.

This study was undertaken while on leave from the Atmospheric Environment Service.

TABLE OF CONTENTS

LIST OF TABLES

LIST OF FIGURES

CHAPTER I

INTRODUCTION

For a long time meteorologists and geographers have been interested in the effect of mountains on weather and climate. One of the more dramatic effects of mountains on weather is the Foehn phenomenon. Other effects have been studied and appear in the literature. Susuki and Yakuki (1956) discussed crop damage and loss of homes in the vicinity of mountains in Japan. The transport of particles by mountain winds has been investigated by Förchtgott (1950). The distribution of precipitation in mountainous regions was considered by Sawyer (1956). Smoke movement and discontinuous spreading of forest fires on slopes have recently been studied by California forestry researchers. The aviation industry is concerned with flying aspects over mountains. The problems of flying over hills with powered or gliding aircraft have long been scrutinized. Numerous reports in the literature attest to the action of turbulence in flight over mountains.

Kuettner (1953) and Queney et al. (1960) have described special safety precautions for aircraft crossing uneven terrain. It has often been reported that flight through mountain waves is remarkably smooth, however, violent turbulence that occurs in

association with these waves can be quite abrupt. Turbulence may occur at any height but the associated complications to flight would be seriously compounded if the region of turbulence was close to the ground.

Current work in mountain effects derives much of its strength from a major study under way at the National Center for Atmospheric Research (NCAR) located in Boulder, Colorado. Lilly (1967) described a massive field program including six aircraft used to measure the airflow over the front range of the Colorado Rockies. Staff at NCAR have used data gathered in this way in an attempt to complete the picture of lee wave properties. Research activities vary from an operational linear lee wave model developed by Vergeiner (1971) to a contribution to wave momentum flux by Lilly (1971).

In Alberta Longley (1967) studied the frequency of chinooks and immediately recognized a problem, still unanswered, as to what precisely constitutes a chinook. It is apparent from other sources that whatever definition best suits the project at hand has been used. This study will not attempt to follow or put forth any rigid definition, but instead will recognize fluctuations in a measured parameter that may at times precede dramatic chinook-type warming.

Glenn (1961) classified chinooks into four types according to the process acting before or during the chinook. One type involves a cold air mass banked against the Eastern slope of the Rocky Mountains. The cold air mass is shallow and some form of disturbance sets up an oscillation along the interface of the boundary between the cold air and warmer air above. Eventually the cold air will be eroded

completely with the warmer air extended down to the surface. Frequently the final stages of the warm air penetration will occur abruptly. This type of penetration has been observed to occur in southern Alberta. It is to further understanding of these events that this study pursues.

A knowledge of the characteristics of these penetrations would be useful in two ways: first, in providing insight into dispersal of urban pollutants through the breakdown of strong inversion conditions in the lower atmosphere, and second, in documenting a possible source of low level turbulence. In the vicinity of airdromes low level turbulence would be particularly important in the critical flight stages of landing and take-off.

A previous study combining airborne measurements over Southern Alberta and Scorer's (1949) lee-wave theory is that of Holmes and Hage (1971). They found evidence of an intermediate wavelength occurring in the winter months of 1967 and 1968 between Calgary and Medicine Hat. The wavelengths observed ranged from 45 to 70 km. Numerical solutions obtained from theory were found to exist for wavelengths of 60-70 km, but the sensitivity of the solution to changes in the mean wind speed suggested that such wavelengths would be rare and of short duration.

Starr and Browning (1972) have used high-power radar to observe the structure of lee waves and found evidence of wavelengths of about 25 km.

Vergeiner and Lilly (1970, Figure 11) show streamfunction lines drawn over a profile of the front range that suggests the

interaction of a short (11 km) lee wave with a longer (50 km) wavelength.

This study is directed toward providing answers to questions about the structure of the lowest levels of the atmosphere prior to and during the surfacing of the warmer air associated with these phenomena. The method of probing these lowest levels was an instrumented 91 m tower located in south-east Calgary, Alberta.

Chapter II contains a detailed description of the data. A full discussion of the method used to calculate variance spectra is presented in Chapter III. Chapter IV is concerned with the results of the study.

CHAPTER II

DATA

2.1 Primary Sources of Data

2.1.1 Bonnybrook (BBRK) Tower

The bulk of the data obtained for analysis consisted of temperature measurements recorded on a 91 m tower located in south-east Calgary near Bonnybrook road and 42nd Avenue. The tower operation was sponsored by the Alberta Department of Public Health and serviced by Geoscience Research Associates Ltd. located in Edmonton.

Continuous records in the form of folded strip charts were acquired for the period 1 November 1970 to 31 March 1971. The temperature was observed at 4 levels on the tower, each level recording the temperature every minute. Different colours of ink were used to distinguish the levels.

Along with the temperature measurements, concurrent wind observations were obtained in roll-chart form. Wind direction and speed were recorded at two levels (1 and 4) on the tower.

Table 1 shows the base elevation and height above ground of the sensors on the tower.

2.1.2 CFCN Tower

A second source of temperature observations was an instrumented television transmission tower 96 m high. This tower was located on Broadcast Hill at the extreme western edge of the city of Calgary. The University of Calgary Weather Research Station was responsible for the observations on the CFCN tower.

Other than the first three months of 1971, intermittent unserviceabilities rendered most of the other periods of record valueless. Temperatures were recorded at four levels on the tower, six times per hour. Printed numbers were used to distinguish between levels.

No measurements of wind were taken on the CFCN tower.

Table 1 lists the base elevation and heights above ground of CFCN tower sensors.

Figure 1 shows the location of the BBRK tower (T1) and the CFCN tower (T2) with respect to the city boundaries.

2.2 Secondary Sources of Data

2.2.1 Fire Halls

Thermographs are maintained by various substation fire halls scattered throughout the city of Calgary. These sites were sponsored by the Alberta Department of Public Health and serviced by Geoscience Research Associates Ltd.

Continuous temperature observations in the form of thermograph strip charts were acquired from seven locations around the city.

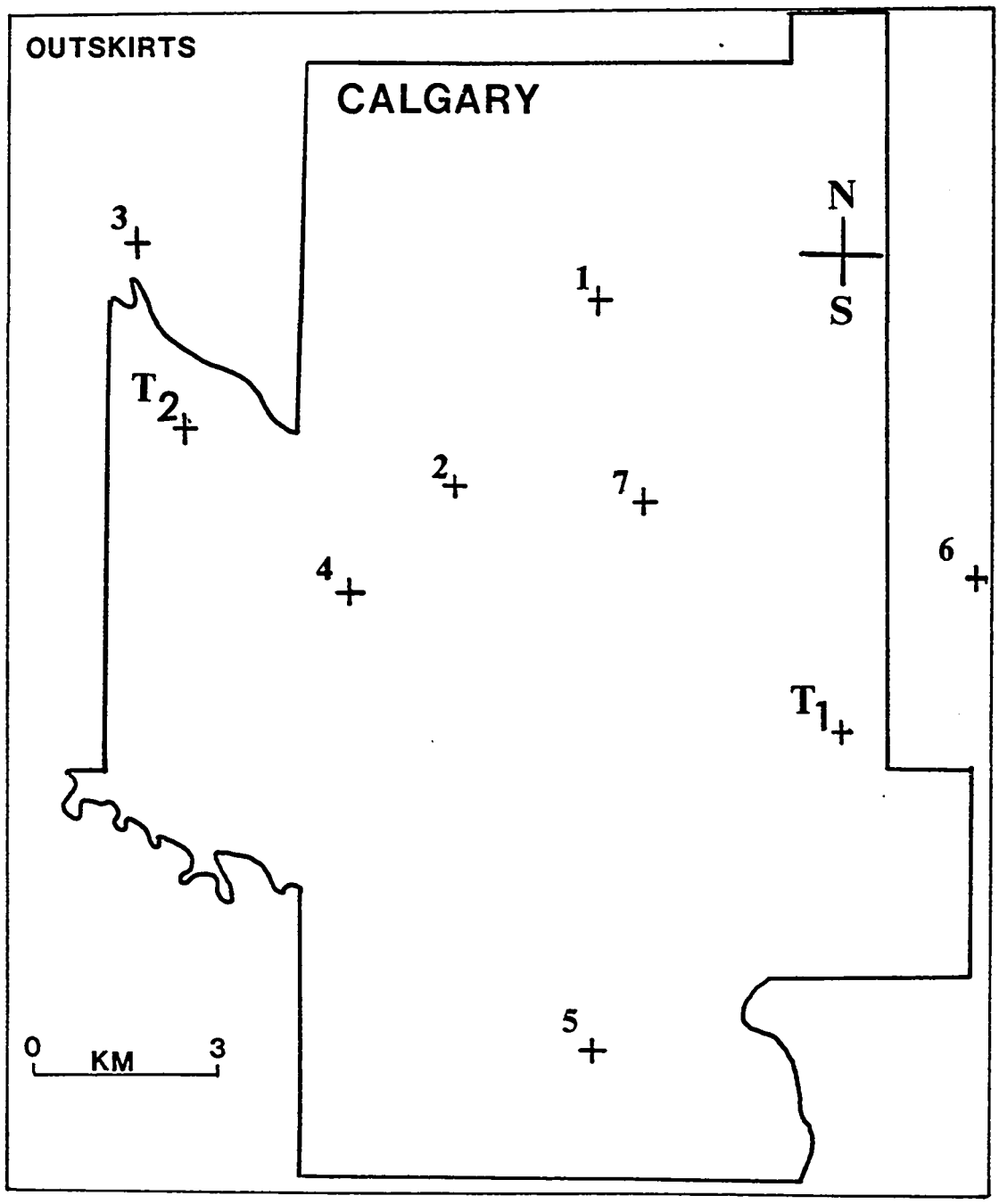

Figure 1. Map of calgary showing the location of the thermograph sites(numbered), the BBRK tower(T_1), and the CFCN tower(T_2).

These records covered the period January to March, 1971 inclusive. Accurate logs of time and temperature corrections were available for each station.

Table 2 lists the thermograph locations in the city.

Table 1

Tower Specifications

Level	BONNYBROOK m[1]	BONNYBROOK ft.[2]	CFCN m[1]	CFCN ft.[2]
base	1028.7	3375	1194.5	3919
1	4.57	15	6.09	20
2	30.4	100	35.1	115
3	60.9	200	65.5	215
4	91.4	300	96.0	315

[1]AGL [2]ASL

Table 2

Thermograph Locations

Station No.	Location
1	4th St. and 26th Ave., N.W.
2	19th St. and Memorial Dr.
3	Bowood Dr. and 63rd St.
4	21st Ave. and 29th St., S.W.
5	McLeod Tr. and 94th Ave.
6	37th St. and 18th Ave., S.E.
7	1st St. and 6th Ave., S.E.

Figure 1 shows the location of each thermograph according to station number.

2.2.2 Chinook Research Stations

Several hygro-thermograph stations were established by the University of Calgary Department of Geography for a chinook research project. Strip charts were obtained for five stations west of Calgary. A detailed description of the station sites can be found in Marsh (1965).

Continuous records were available for the period 1 November 1970 to 2 February 1971, when operation of the stations ceased. A sixth station, located on the campus of the University of Calgary, had continuing records through April, 1971.

These stations monitored the surface temperature and humidity continuously. Unfortunately no log of time or temperature corrections was available, thus the value of these records was decreased. Table 3 lists these stations by name and gives the distance away from the campus station as measured along an east-west line through the campus location.

Figure 2 shows the locations of the chinook stations according to station number as listed in Table 3.

Table 3

Chinook Station Distances

Station No.	Station Name	Distance (km)
1	Campus	-
2	Mink	8.8
3	Cochrane	15.0
4	Hilltop	35.8
5	Copithorne	41.4
6	Hector	63.0

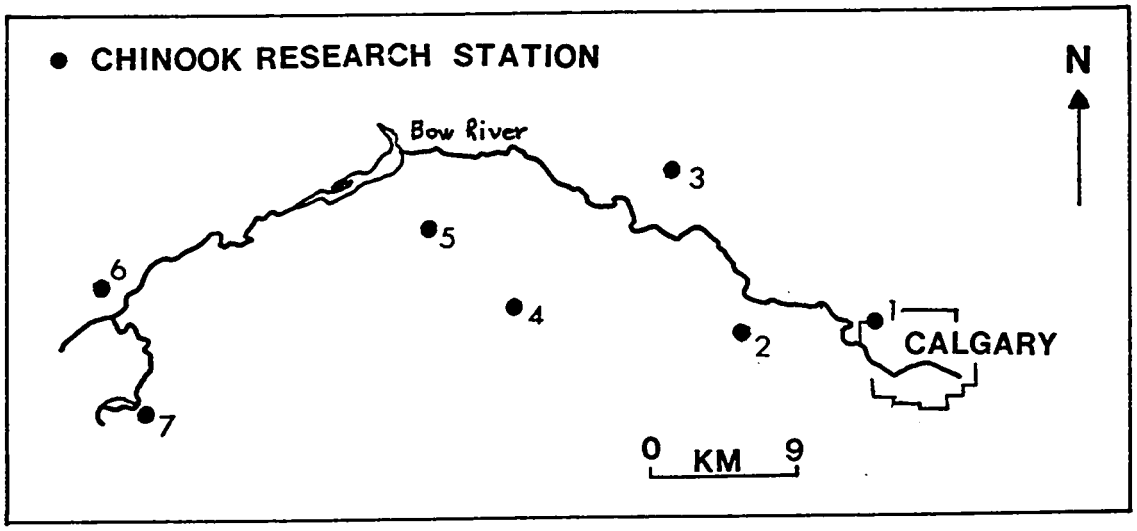

Figure 2. Map of area west of Calgary showing the locations of the Chinook Research Stations.

2.3 Selection of Data Samples

The temperature records from the BBRK tower were examined visually in order to choose samples for further analysis. The type of events selected involved abnormal temperature fluctuations at one or more levels on the BBRK tower. Of particular interest were occurrences of these temperature fluctuations that were followed by a complete removal of the cold air at the surface.

A certain amount of bias may have been introduced in the selection and rejection of samples. Twelve samples were chosen. There were 37 instances of large or abnormal temperature fluctuations out of which 33 showed chinook-type surface warming. Eleven of the 12 samples chosen exhibited this warming. Twelve out of the 37 samples showed a return of the cold air. Seven of these were included in the study.

Table 4 contains a chronological list of the samples taken from the BBRK tower. Included in the list are the initial and final times for each sample, the length in hours, and the total number of points in each sample.

2.4 Upper Air Analysis

Through the courtesy of the Edmonton Public Weather Office an inspection of the upper air analysis charts was performed for the days corresponding to the 12 samples chosen.

Table 4

Cases Under Study

Date	Initial MST.	Final MST.	Duration Hours	Duration Points
13-14 Nov. 70	132100	140730	10.5	630
23-24 Nov. 70	231430	240100	10.5	630
5-6 Dec. 70	051900	061300	18.0	1080
10 Dec. 70	100100	100930	8.5	510
14 Dec. 70	140530	141030	5.0	300
15-16 Jan. 71	151730	160930	16.0	960 *
26 Jan. 71	261600	262100	5.0	300 *
1 Feb. 71	011730	012130	4.0	240 *
11-12 Feb. 71	111930	120930	14.0	840 *
21 Feb. 71	211830	212300	4.5	270 *
1-2 Mar. 71	012100	020900	12.0	720 *
28-29 Mar. 71	281930	290130	6.0	360

* concurrent data samples obtained for the CFCN tower

2.4.1 Upper level winds

Table 5 lists the 700 mb and 500 mb winds for southern Alberta as extracted visually from the charts.

Table 5

Upper Winds

Case	700 mb wind (kts)	500 mb wind (kts)
1	270/20	250/40
2	250/50	250/65
3	260/45	260/55
4	275/15	280/20
5	270/20	250/35
6	250/40	270/45
7	280/40	280/45
8	290/35	270/45
9	300/25	300/60
10	240/20	250/25
11	270/30	330/40
12	270/25	280/35

All cases showed a moderate to strong westerly component usually with an increase in speed at the higher level.

2.4.2 Atmospheric Soundings

Radiosonde ascents were not available for Calgary so that in order to establish a qualitative estimate of the temperature profile the ascents at Edmonton, Alberta and Great Falls, Montana were considered.

For all sample days the profiles showed stable lapse rates. The depth and strength of the lowest inversions varied from very deep and strong (95 mb and 17 C) to shallow (15 mb and 3 C).

2.5 Data Preparation

In order to proceed further with the analysis, it was necessary to transform the data into a form that could be read into a computer.

The strip charts of raw data from both towers represented temperatures recorded in digital form. The major task in preparation of these data was transcribing the digital points onto coding sheets and keypunching computer cards.

Whenever data are abstracted by the same researcher who is going to perform the analysis, it is very difficult to avoid bias. For this reason each case was transcribed level by level, with each level completely transcribed at one time. This procedure was an attempt to maintain, if not a minimum amount of bias, at least a consistent bias in each level. Because the variation in temperature from point to point was considered to be the important quantity rather than the absolute temperature, it was felt that this procedure would provide the most accurate data samples.

The temperature scale on the BBRK charts was 10 F per inch, and individual points were distinguishable to at least the nearest 0.25 F. A similar degree of accuracy was possible for the CFCN data. The temperature scale on these charts was 10 F per inch.

The time scale on the BBRK tower was one hour per inch and on the CFCN tower 1 hour per eight inches.

Figure 3 shows a computer drawn plot of the portion of a data sample that was digitized. The time scale is read from left to right and corresponds to local time as read from the data record.

Figure 4 is a trace of a data sample from the BBRK tower for 23-24 November 1970. Local midnight corresponds to hour 10 in the figure and heights to which each trace corresponds are marked. The portion of the trace marked penetration represents the breakdown of the inversion. The return of the cold air is also marked.

In all, almost 30,000 points representing 114 hours of record spaced over 12 cases of varying length were transcribed.

2.6 Description of a Typical Event

This description is not meant as a rigid definition of the occurrence or nonoccurrence of a chinook but more as a synopsis of some of the more obvious features that were readily identifiable from the selected samples.

From the data recorded at both primary sites the following features were identified:

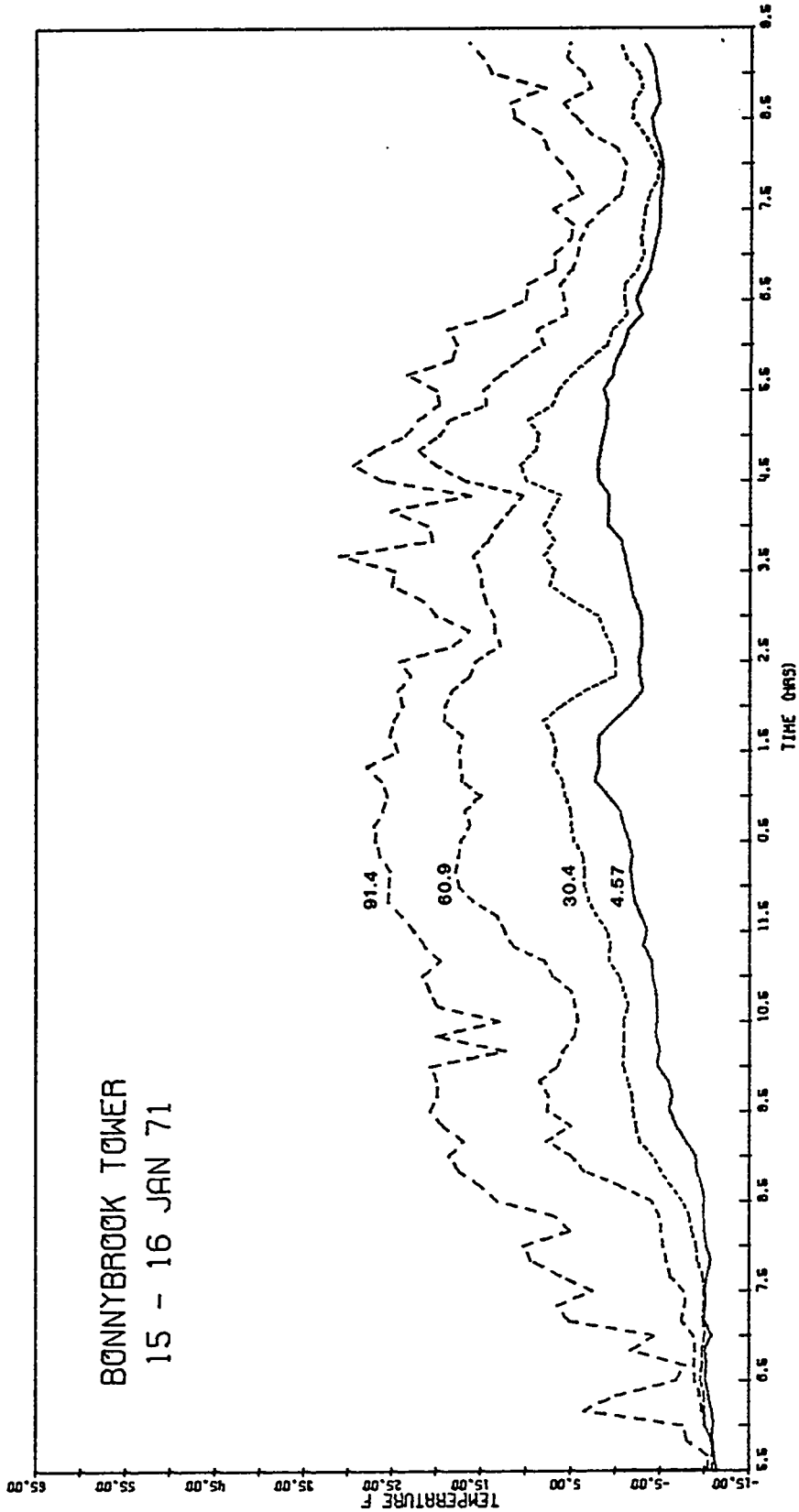

Figure 3. Computer-drawn sample plot of digitized data for Case 6. Time is in local mountain standard and is read from left to right.

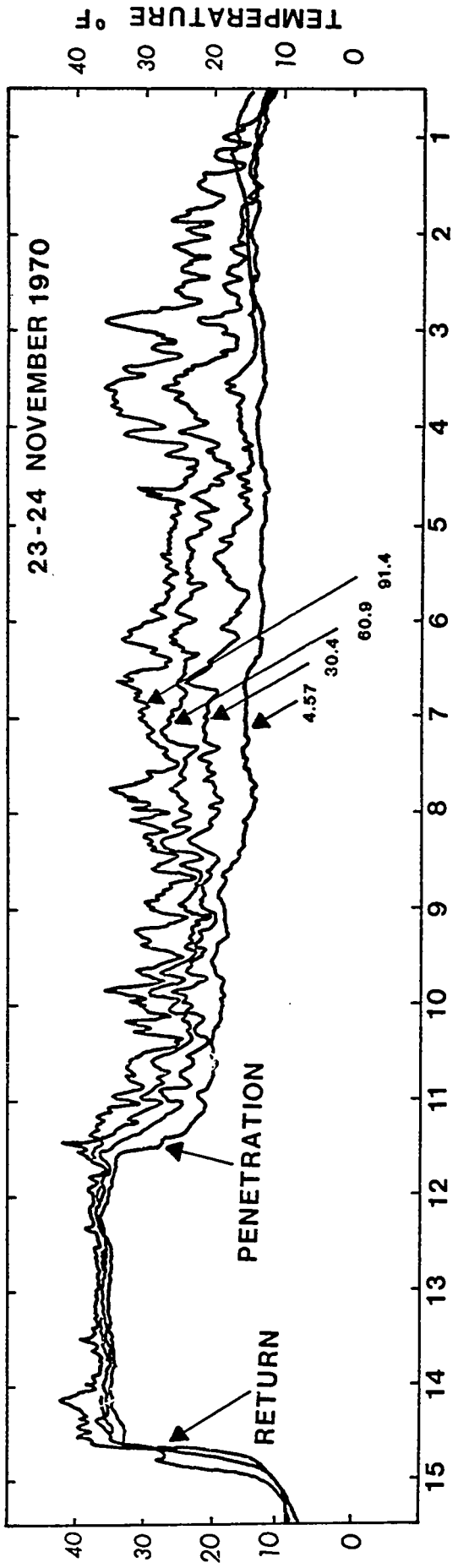

Figure 4. Sketch of typical event taken from the BBRK data. Abnormal fluctuations in the temperature are evident. Inversion breakdown is marked(penetration) and the return of the cold air is marked(return). Hour 10 corresponds to midnight local time.

(i) the temperature fluctuations occurred first at the highest level on the towers and gradually progressed down. Successively lower levels of the tower recorded the oscillations after the level immediately above.

(ii) the fluctuations generally continued for varying periods until the cold air was completely eroded. Subsequent to the cold air withdrawal, all levels of the towers recorded rises in temperature and the oscillations often ceased.

(iii) the temperature rise leveled off and was often followed by a later return of the cold air. A sharp decrease (as much as 45 F in 8 min) accompanied the return.

(iv) as the cold air was eroded the wind speed at the lowest level of the BBRK tower was generally very light. Just previous to and during the rapid temperature increase the mean wind speed increased and exhibited frequent gusts. The direction of the wind was westerly as the speed increased.

(v) at the upper level of the BBRK tower the wind speed remained relatively uniform, with moderate gusts. During the breakdown of the cold air, the mean speed increased and peak gusts occasionally reached 30 m sec^{-1} (60 mph). The general direction was westerly.

(vi) as the cold air returned, wind directions at both levels shifted toward the north.

The two towers did not give equally detailed descriptions because of the different sampling frequencies. The BBRK tower yielded 10 times the resolution of the CFCN tower. There was, however,

sufficient detail in the CFCN record to confirm that the same events were being recorded at the two sites. A visual comparison of plots of the raw data was used to support this conclusion. For the BBRK data only every tenth point was plotted in order that both traces would contain the same number of points.

This qualitative description augments the quantitative description given in Holmes and Hage (1971). Figure 5 taken from Holmes and Hage (1971) shows mean values of vertical shear of the horizontal wind and vertical temperature gradient at times relative to inversion breakdown.

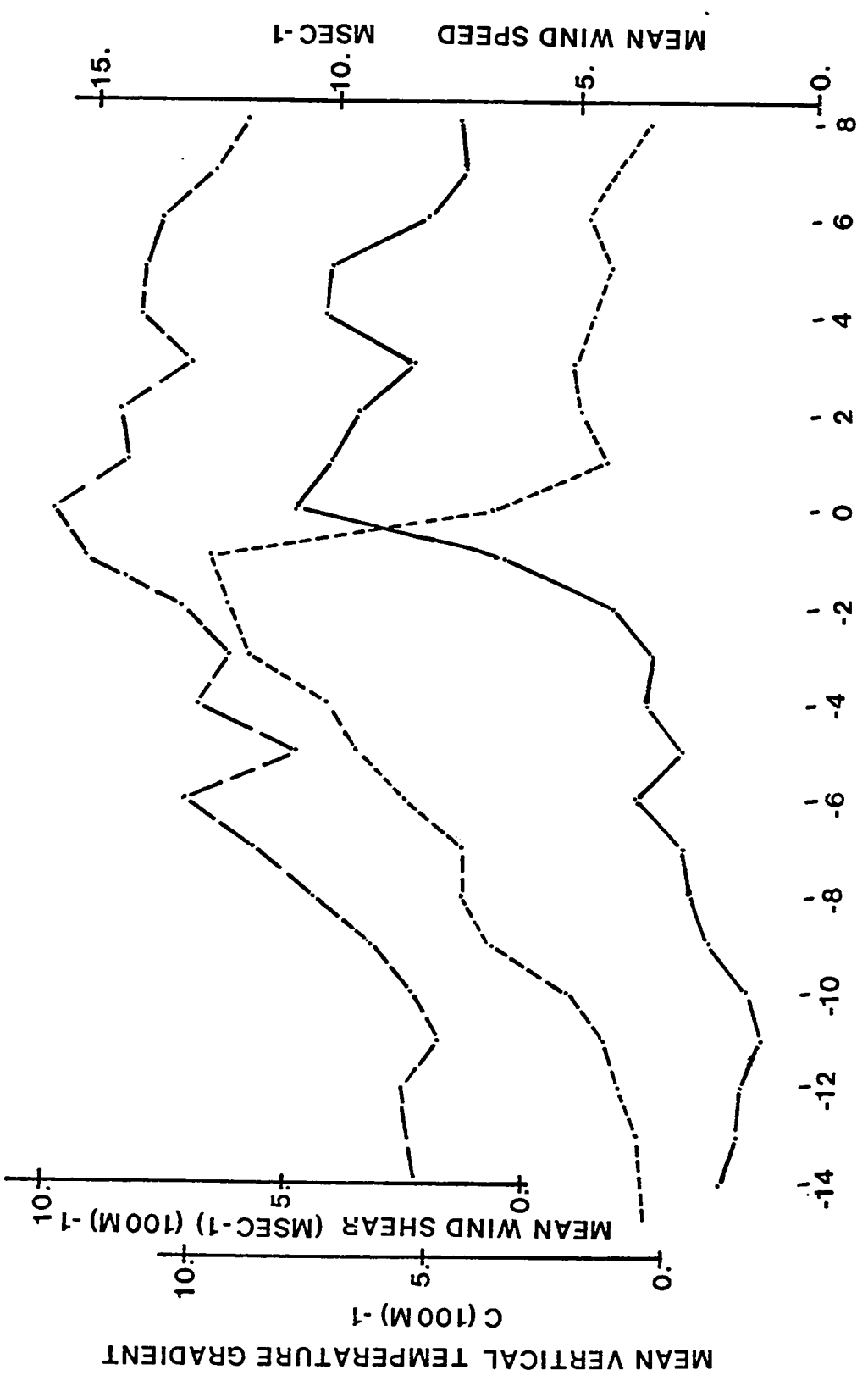

Figure 5. Average values of the vertical shear of the horizontal wind speed, vertical temperature gradient and mean wind speed for six occurrences of warm air penetration to the surface at Calgary. (taken from Holmes and Hage 1971)

CHAPTER III

METHOD OF ANALYSIS

3.1 Introduction

The primary data samples consisted of sequential temperature values measured at equally-spaced intervals in time. Inspection revealed fluctuations in temperature that resembled wave activity in the atmosphere. In order to investigate the wave structure from a statistical viewpoint the technique of variance spectrum analysis was applied.

3.1.1 Selection of a method

Two methods were considered. The first, outlined by Blackman and Tukey (1959), involves computing an autocovariance function for each sample. This method has an advantage in being readily adaptable to samples that vary in length. An autocovariance can be calculated to the same lag expressed as a percentage of the total sample size in each sample, thereby maintaining a consistent stability throughout the analysis. The second method involves computing a modified periodogram. This method is the classical approach of Shuster (1900). Since the advent of the fast Fourier transform (FFT) algorithm in 1965 this method has been rediscovered. The periodogram by itself has a distinct lack of stability but by averaging large numbers of

samples the stability is added to the periodogram. For large numbers of moderately long records this method is particularly adaptable to a routine analysis.

The 12 samples chosen for analysis from the BBRK tower varied in length from 240 to 1080 points. Because of the record length and relatively small number of samples the autocovariance method seemed to be the proper choice. After several pilot studies described by Kellie (1972), and after a comparison between the results of the two methods, it was apparent that the periodogram technique provided more useful results. Table 6 gives a comparison of low frequency results for the two methods from the pilot study. The pilot series were temperature measurements in which the amplitude of a low frequency diurnal fluctuation was much larger than the superposed fluctuations that were of interest.

Table 6

Low Frequency Results

Frequency	Variance via Autoco.	Variance via Periodogram
0	3.070	0.370
1	0.713	1.263
2	0.327	1.520
3	0.020	0.822
4	0.145	0.653

Of note is the fact that the results of the autocovariance method were dominated by the diurnal fluctuation. The contribution of this long wavelength appeared as a trend in frequency zero and essentially overpowered the variance contributions of the frequencies of interest. The periodogram method does not show these characteristics. On the basis of this comparison a decision was made to proceed with the periodogram approach.

3.2 Averaged Modified Periodograms

3.2.1 Variance Spectra

Let X_i , $i = 1, \ldots, N$ be a second order, weakly-stationary sequence of observations measured at equally-spaced intervals of time. The variability is characterized by the variance which can be estimated by

$$s^2 = \frac{1}{N-1} \sum_{i=1}^{N} (X_i - \mu)^2 \qquad (3.1)$$

The expected value is characterized by the mean

$$\mu = \frac{1}{N} \sum_{i=1}^{N} X_i \qquad (3.2)$$

which is assumed constant. The simplest multivariate moment is characterized by the covariance between values of X(t) at different times and is estimated by

$$C_{xx}(\tau) = \frac{1}{N} \sum_{i=1}^{N} X_i \cdot X_{i+\tau} \qquad (3.3)$$

The periodogram, I(n), is the Fourier transform of $C_{xx}(\tau)$

$$I(n) = \sum_{j=1}^{N} C_{xx}(\tau) \exp(-i\, 2\pi\, jn/N) \qquad (3.4)$$

$$n = 1, \ldots, N$$

The underlying assumption being that of weak stationarity has been discussed by Jenkins (1961). Weak stationarity means that the statistical moments up to second order depend on differences $(t_i - t_{i+\tau})$ rather than on t_i or $t_{i+\tau}$ themselves. If an additional assumption is made that the statistical properties of X(t) are governed by a Gaussian process, then s^2, m and $C_{xx}(\tau)$ characterize the statistical behaviour of X(t) completely.

An equivalent description for the covariance is provided by the power spectrum which is the Fourier transform of the covariance function.

$$P(n) = \frac{1}{N} \sum_{j=1}^{N} C(\tau) \exp(-i\, 2\pi\, jn/N) \qquad (3.5)$$

$$n = 1, \ldots, N$$

The periodogram describes how the variance is distributed with frequency.

Variance spectra of temperature were calculated using a method described in detail by Welch (1967). The method involves dividing the record into sections and calculating a modified periodogram for each section. The power spectrum is obtained by averaging the periodograms. A summary of the method is also presented in Steenbergen (1971).

Each sample was divided into K segments, $X_k(j)$, k=1,..., K consisting of L points overlapping by one-half their length. In this study L was 128.

The mean and a linear trend were removed from each segment. Bendat and Piersol (1966) described a method to estimate the trend. The first third and last third of each segment were averaged and these averages were used to estimate the linear trend.

Welch (1967) suggested multiplication by a data window W(j), that has a shape $1 - |t|^2 : -1 \leqslant t \leqslant 1$ where

$$t = \left\{ \frac{j - \frac{L-1}{2}}{\frac{L+1}{2}} \right\} \qquad (3.5)$$

A plot of this window reveals a shape close to that of a Hanning cosine bell. Thus a new sequence was formed from each data block through multiplication by a Hanning data window W(j)

$$W(j) = \frac{1}{2}(1 - \cos 2\pi j/L) \qquad (3.7)$$

$$j = 0,1, \ldots, L-1$$

$$= 0 \quad \text{otherwise.}$$

Bingham, Godfrey and Tukey (1967) showed that a Hanning window used as a data window before the Fourier transformation falls off at least as rapidly as $|n - n_j|^{-2}$ as n_j recedes from n. This characteristic reduces the problem of leakage.

The spectral window corresponding to the Hanning data window is given by

$$Q(n) = U^{-1} \left| L^{-1} \sum_{j=0}^{L-1} W(j) \exp(-i\, 2\pi\, jn/L) \right|^2 \quad (3.8)$$

where

$$U = L^{-1} \sum_{j=0}^{L-1} W^2(j) \quad (3.9)$$

Cooley, Lewis and Welch (1969, Fig. 7) gave a plot of the spectral window which showed the reduction in side lobes. The value of U for the Hanning data window was approximately 3/8. When the area under the spectral window was normalized to unity the half-width of the spectral window was 0.8 and the height of the first side lobe was 6×10^{-4} times the height of the main lobe.

A discrete Fourier transform was performed on all segments

$$A_k(n)_x = L^{-1} \sum_{j=0}^{L-1} X_k(j)\, W(j) \exp(-i\, 2\pi\, jn/L) \quad (3.10)$$

$$k = 1, \ldots, K$$

$$n = 0, \ldots, L/2$$

The frequency, n, was expressed as cycles per unit time, where the unit of time was the length of one segment of the sample, or 128 min.

The Fourier transform was performed using a Fast Fourier Transform (FFT) subroutine available in the University of Alberta program Library. The algorithm, written by G. Sande was described in detail by Cochran et al. (1967). The length of the series, L,

must be an integral power of 2.

$$I_k(n)_x = 2U^{-1} |A_k(n)_x|^2 = \sqrt{a_k^2 + b_k^2} \qquad (3.11)$$

Division by U corrected the variance for the effect of pre-multiplication by the data window. The factor of 2 arises from the definition of spectral estimates in terms of positive frequencies only.

The spectral estimates were obtained by averaging the periodograms

$$P_x(n) = K^{-1} \sum_{k=1}^{K} I_k(n)_x \qquad (3.12)$$

3.2.2 Cross-spectra

If $X_i(j)$ $i = 0,1, \ldots, N-1$ and $Y_i(j)$ $i = 0,1, \ldots, N-1$ are time sequences both measured over the same period then an estimate of the cross covariance $C_{xy}(\tau)$, is given by

$$C_{xy}(\tau) = N^{-1} \sum_{j=0}^{N-k-1} X(j+k)\ Y(j) \qquad (3.13)$$

$$0 \leqslant k < N$$

and the cross periodogram $I_{xy}(n)$ is the Fourier transform of $C_{xy}(\tau)$

$$I_{xy}(n) = \sum_{j=0}^{N-1} C_{xy}(\tau) \exp(-i\, 2\pi\, jn/N) \qquad (3.14)$$

$$n = 0, \ldots, N-1$$

Each cross-spectral estimate involved two levels of tower data, thus for each sample day there were six possible combinations.

The cross spectra were estimated in a fashion completely analogous to that for variance spectra of the individual levels.

Data from a pair of levels were divided into K segments each of length L, $X_1(j)$, ..., $X_k(j)$ and $Y_1(j)$, ..., $Y_k(j)$. The mean and a linear trend were removed in the same manner as previously discussed. The Hanning data window was applied to each section followed by a discrete Fourier transform.

$$A_k(n)_x = L^{-1} \sum_{j=0}^{L-1} X_k(j)\, W(j) \exp(-i\, 2\pi\, jn/L) \tag{3.14}$$

$$A_k(n)_y = L^{-1} \sum_{j=0}^{L-1} Y_k(j)\, W(j) \exp(-i\, 2\pi\, jn/L) \tag{3.15}$$

$$n = 0,1, \ldots, L-1$$

$A_k(n)_x$ and $A_k(n)_y$ being complex numbers can be separated into real and imaginary parts

$$A_k(n)_x = a_x + ib_x \tag{3.16}$$

$$A_k(n)_y = a_y + ib_y \tag{3.17}$$

The cross periodogram for each pair of segments was defined as

$$I_{xy}(n)_k = 2U^{-1}\, \tilde{A}_k(n)_x \cdot A_k(n)_y \tag{3.18}$$

where $\tilde{A}_k(n)_x$ was the complex conjugate of $A_k(n)_x$. Separating equation (3.18) into real and imaginary parts

$$R_e(I_{xy}(n)_k) = 2U^{-1}(a_x a_y + b_x b_y) = C_{xy}(n)_k \tag{3.19}$$

$$I_m(I_{xy}(n)_k) = 2U^{-1}(a_x b_y - a_y b_x) = Q_{xy}(n)_k \tag{3.20}$$

$C_{xy}(n)_k$ is known as the cospectrum which is a measure of the cross covariance for zero phase angle between the two series. $Q_{xy}(n)_k$ is known as the quadrature spectrum, which is a measure of the cross covariance for a 90 degree phase relationship.

The cospectral and quadrature spectral estimates were obtained by averaging

$$C_{xy}(n) = K^{-1} \sum_{k=1}^{K} C_{xy}(n)_k \tag{3.21}$$

$$Q_{xy}(n) = K^{-1} \sum_{k=1}^{K} Q_{xy}(n)_k \tag{3.22}$$

From the averaged values given by Eqs. (3.21) and (3.22) the cross-periodogram estimates were formed

$$P_{xy}(n) = C_{xy}(n) + i\, Q_{xy}(n) \tag{3.23}$$

A measure of the correlation between the amplitudes of the two series at any particular frequency can be found from the coherence spectrum

$$COH_{xy}(n) = \frac{|P_{xy}(n)|^2}{P_x(n) \cdot P_y(n)} \tag{3.24}$$

$$0 \leq COH_{xy}(n) \leq 1$$

The coherence spectrum considers correlations between the two levels in narrow frequency intervals.

The phase lag between levels at particular frequencies is given by

$$TH_{xy}(n) = \arctan\left(\frac{Q_{xy}(n)}{C_{xy}(n)}\right) \qquad (3.25)$$

$TH_{xy}(n)$ was calculated in terms of fractions of a circle in radians. The quadrant of the phase angle can be determined from the signs of $C_{xy}(n)$ and $Q_{xy}(n)$ which represents the real and imaginary parts of Eq. (3.18).

3.3 Confidence Limits

In this type of analysis it was desirable that variance spectrum estimates that appeared significant were declared significant with a minimal chance of a type 2 error. The null hypothesis H_o was expressed as

> H_o: the variance at a frequency, n, is significant if its value exceeds the 95 per cent confidence band.

Rejection of H_o implies acceptance of the alternative.

The hypothesis that was adopted was that the variance at a particular frequency was a random fluctuation of the population variance. A variance that is distributed equally among all frequencies is commonly referred to as white noise.

3.3.1 Variance Spectra

Because of variations in the stability, consideration of the variance at any frequency for the purpose of acceptance or rejection of a hypothesis may not be the best method of interpretation. Consistency in the shape of the spectral curve from sample to sample may be more important. In order to reduce the samples to a common base a white noise hypothesis was made and the spectral estimates were normalized. The procedure for normalizing the variance spectra has been described in detail by Eddy, Duchon and Almazon (1968). If the white noise hypothesis was upheld the process under study would represent random fluctuations for which the variance spectrum should be distributed equally flat or independent of frequency.

Each variance estimate was divided by $(2\hat{\sigma}^2/m)$, where $\hat{\sigma}^2$ is an estimate of the population variance and m is the Nyquist or folding frequency, 64 cycles in 128 min., in this study.

The ratio of the sample variance to the population variance is distributed as ψ^2/ν, where ν is the effective degrees of freedom. Estimates of the sample variance are not independent because of blurring created by the window. Therefore, the number of degrees of freedom depends upon the choice of window. For this study, a Hanning window was applied and the effective number of degrees of freedom was 2N/M, where N is the record length and M is the maximum lag (block size 128). One was subtracted from ν to take into account the fact that the population variance was estimated from the data sample.

The confidence bands for 95 per cent and 5 per cent levels were added to the graphs of normalized variance. The interpretation

placed on these limits was that the probability of spectral estimates exceeding the 95 per cent confidence limit was 5 per cent and the probability of the estimate being less than the 5 per cent limit was 5 per cent. Any estimate falling within the confidence band had a 90 per cent chance of being no different than a random fluctuation.

3.3.2 Cross-spectra

Confidence limits were plotted for the spectra, cospectra, quadrature spectra, and cross-spectra in a manner completely analogous to that used for the variance spectra. The number of degrees of freedom did not change.

3.3.3 Coherence

The coherence as calculated from Eq. (3.24) is analogous to the Pearson correlation coefficient. Fisher (1958) showed that a transformation.

$$z' = \arctan |COH_{xy}(n)| = \frac{1}{2}\ell n \left(\frac{1 + |COH_{xy}(n)|}{1 - |COH_{xy}(n)|}\right) \qquad (3.26)$$

results in a new variable z' that is approximately normally distributed with variance equal to $1/\nu$. The degrees of freedom, ν, are the same as those for the variance spectrum. The confidence limits are $\pm\alpha(\%)\sqrt{1/\nu}$, where $\alpha(\%)$ can be found from a normal table for the desired percentage probability level. For this study $\alpha(95) = 1.96$ was used. The 95 per cent confidence limit was plotted on graphs of the coherence transformed to a Fisher z' variable.

CHAPTER IV

RESULTS

Variance spectrum results are expressed as functions of frequency, n, where frequency is defined in terms of cycles per unit time. In this study the time unit was the length of one data segment, or 128 min. The variance is expressed in non-dimensional form in which the power was normalized (by $2\hat{\sigma}^2/m$) under a white noise hypothesis. This form of presentation was chosen to facilitate visual comparisons, in that it represents a method of reducing a large number of spectral plots to some common base.

Plots of variance spectra presented in the Appendix are labelled according to date and height. Pilot spectra examined in a previous study by the author were displayed for the frequency range zero to the Nyquist frequency, 64 cycles per 128 min. These results indicated that the variance decreased by at least two orders of magnitude, typically 10^{-1} to 10^{-4}, in frequencies higher than 20 cycles per 128 min. For this reason graphs of variance spectra were truncated at frequency 32 cycles per 128 min.

4.1 Variance Spectra Results

The plots of variance spectra for the individual levels from the BBRK tower are presented in the Appendix (Figures A-1 to A-10). A sample plot is shown in Figure 6.

The general shape of the spectra is considered to be the significant feature common to these graphs. Minor variations in the general shape from case to case although not necessarily insignificant, are thought to be representations of microscale activity perhaps induced by the urban environment that surrounds the BBRK tower.

The overall shape of the spectral estimates was the same for all samples. All spectra exhibited a peak at low frequencies. A large percentage of the power was concentrated in low frequencies with a rapid decrease in variance over a narrow range of intermediate frequencies. The highest frequencies contained little power. Variance estimates in these frequencies were at least two orders of magnitude smaller than those at low frequencies. This shape was consistent throughout the entire 48 samples (12 cases, each with 4 levels), demonstrating that the samples exhibited some degree of homogeneity in the scales of the temperature fluctuations. Furthermore, the spectra demonstrated that the temperature fluctuations were not completely random.

No systematic differences between the spectral estimates were evident. Consequently, variations in the shape between samples were attributed to micro-scale activity.

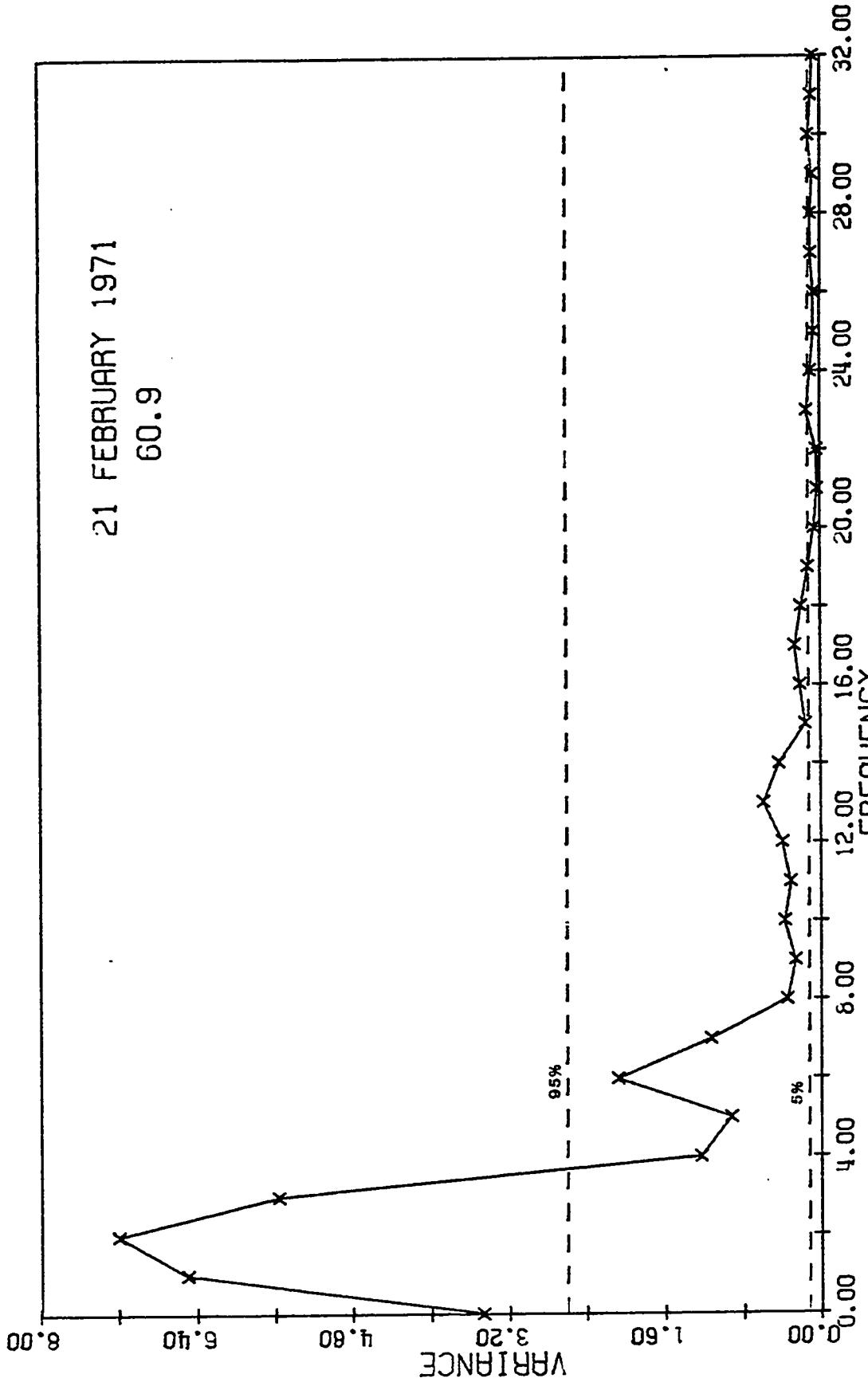

Figure 6. Variance spectrum of temperature. Normalized variance versus frequency (cycles per 128 min.).

4.2 Cross-Spectral Results

Complex cross-spectra (from the BBRK tower) are also displayed as non-dimensional variances against frequency. The complex cross-spectra consisted of cospectral estimates, quadrature spectra and cross-spectra. Figure 7 shows a sample of a cospectral plot. Further cross-spectral plots are displayed in the Appendix (Figures A-11 to A-18). Each figure is labelled with the appropriate data and combination of levels for the sample from which the variance was estimated.

Here too, the overall spectral shape was considered to be the most significant feature. The cross-spectral results exhibited the same shape as the spectra, a large contribution to the variance at low frequencies, a rapid decrease in variance with increasing frequency and much smaller contributions to the variance at high frequencies.

The similarity of the spectra for the individual levels is reflected in the shape of the cross-spectral plots. The results demonstrate that the events measured at the top of the tower were similar to those measured at the bottom.

4.2.1 Coherence Results

The Fischer z'-transformation of coherence estimates are shown in Figures 8 and 9. A coherence spectrum measures the amplitude correlation between levels at the same frequency. At a 95 per cent significance level the low frequencies show coherence values that were significant. These significant estimates were considered to be

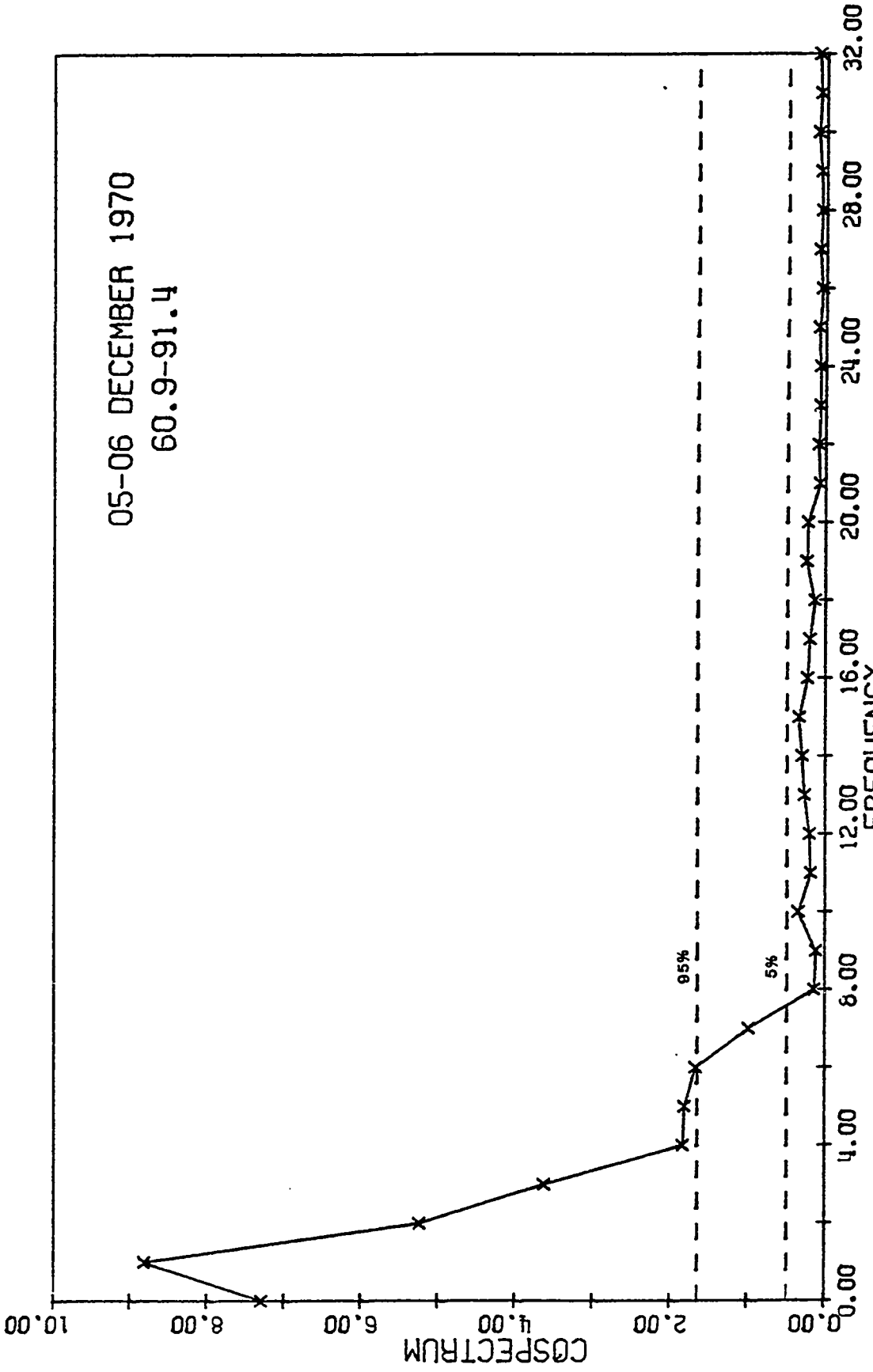

Figure 7. Cospectrum of temperature. Normalized cospectrum versus frequency (cycles per 128 min.).

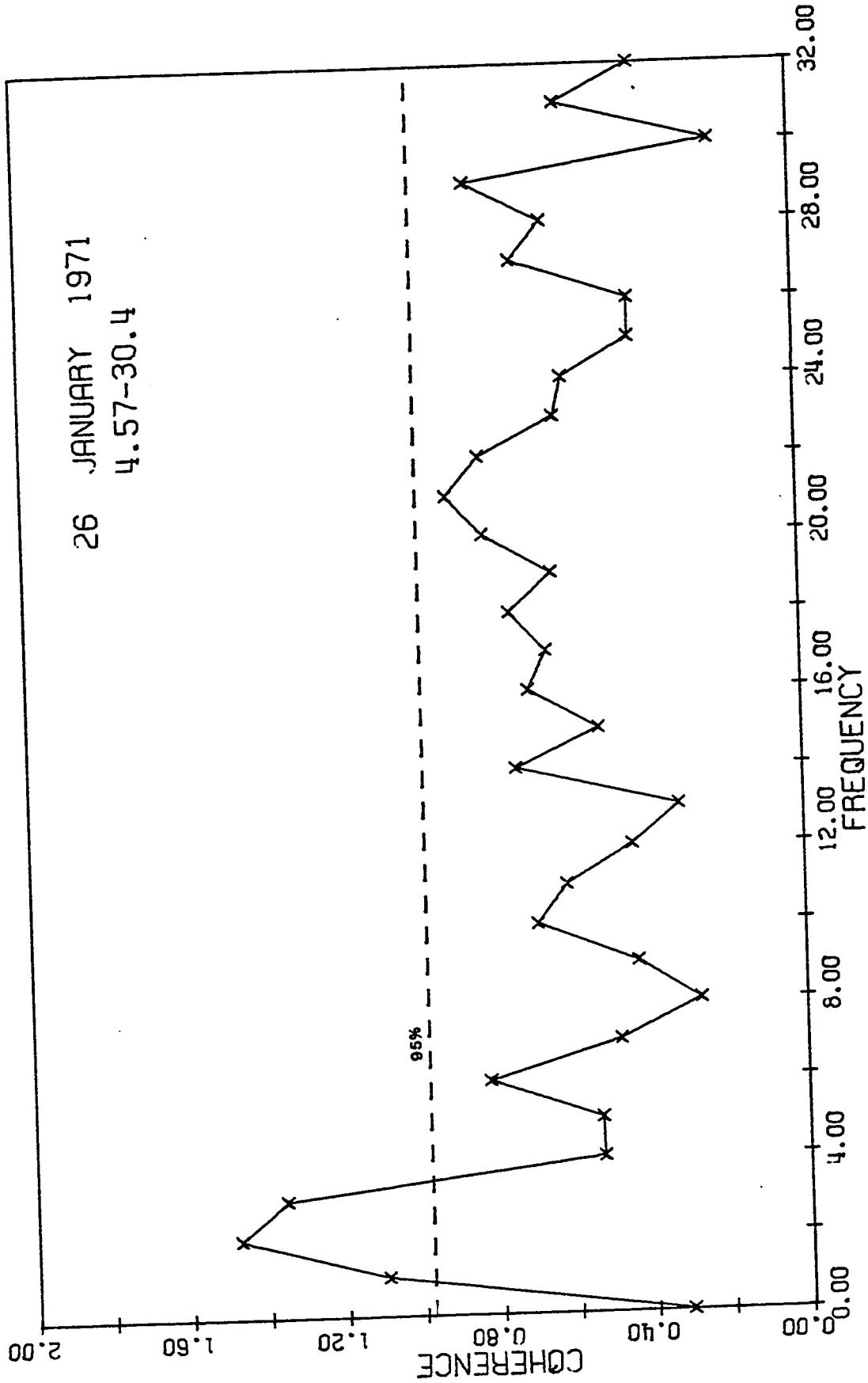

Figure 8. Graph of Fisher z' transformation of coherence versus frequency (cycles per 128 min.).

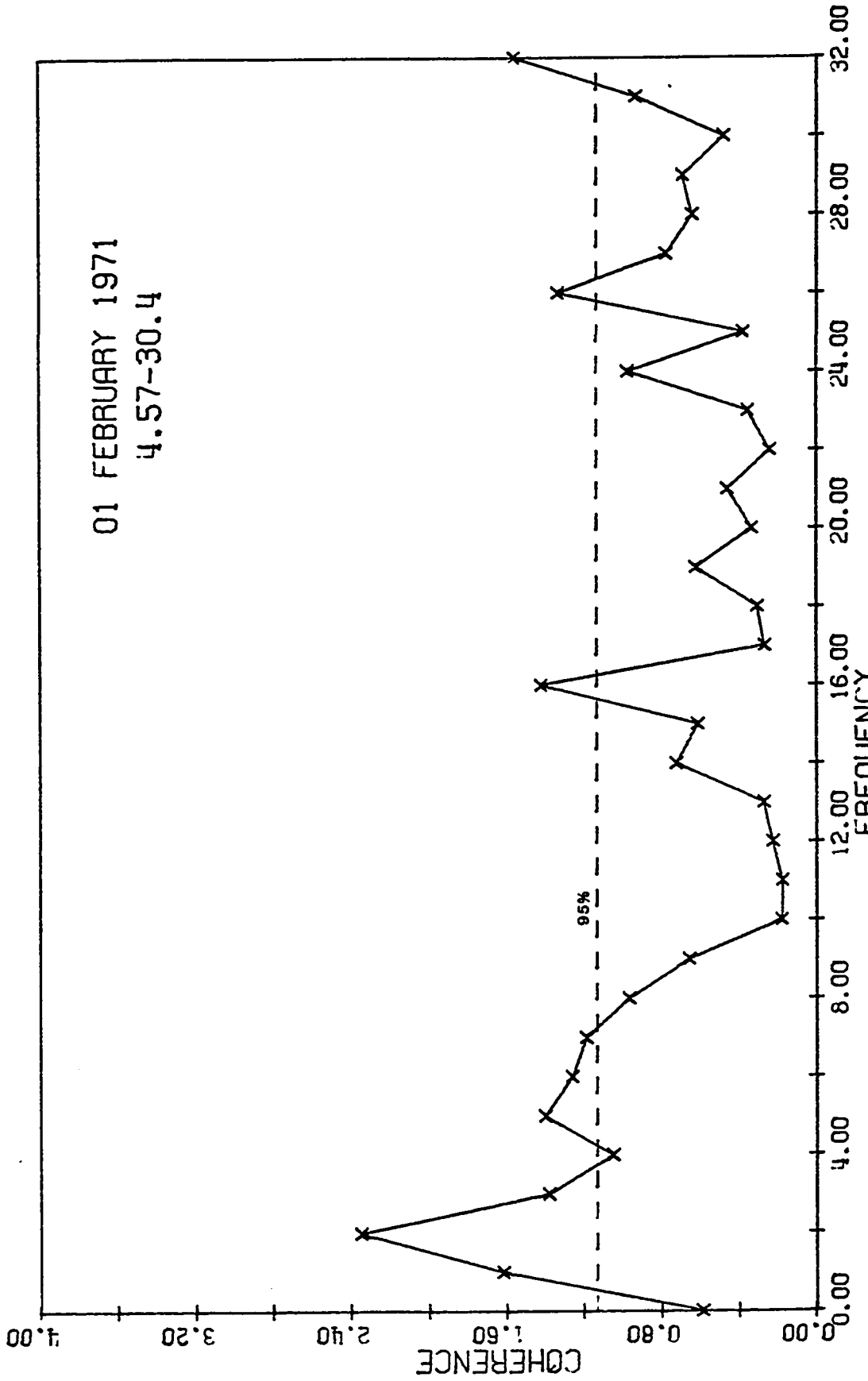

Figure 9. Graph of Fisher z' transformation of coherence versus frequency (cycles per 128 min.).

a reflection of the dominance of low frequencies in the individual spectra. Occasionally coherence values were significant at high frequencies. These values were regarded as significant correlation between small amplitude values. This correlation occurring at high frequencies might be large but the contribution of high frequencies to the variance was small compared to low frequencies. For this reason no significance was attached to apparently-significant high frequency coherence estimates.

4.2.2 Phase Relations

Phase spectra were calculated as functions of frequency for the BBRK tower data. It was hoped that phase relations of the temperature fluctuations with respect to the 91 m level would reveal some of the structural properties. Visual inspection of the data had suggested that the progression of the warm air down the tower would show a discernible time lag from level to level. The results, however, were inconsistent. The phase spectra even at low frequencies displayed characteristics of noise. The phase oscillated about zero and for some samples sign changes were recorded at different levels. Two hypotheses were proposed to explain this inconsistency.

The first alternative is that the levels measured oscillations essentially acting in unison. That is, the phase differences between the top and various lower levels could not be resolved by analysis.

A second alternative was that the phase changes at any particular frequency were obscured by averaging. If the phase

relations had been calculated for shorter time intervals that included only observational periods in which the oscillations were well defined visually, it is suggested that significant results would have been obtained. Regretfully this question must be left open for the present.

4.3 Brunt-Vaisala Frequencies (BVF)

One question that had to be answered was whether or not the observed oscillations corresponded to natural frequencies in the atmosphere. The variance spectra indicated that low frequencies were the major source of variance.

The inertial frequency in the atmosphere is given by the Coriolis parameter $f = 2\Omega \sin \phi \simeq 10^{-4}$ sec^{-1} where Ω is the angular velocity of the earth and ϕ is the latitude. The corresponding period is about 28 hours. The natural frequency for vertical oscillations corresponds to the BVF defined as

$$N^2 = g \frac{\partial \ell n \theta}{\partial z} \tag{4.1}$$

where θ is the potential temperature, and z the height.

Concurrent observations of station pressure were not readily available. Therefore the calculation of the vertical gradient of potential temperature was performed using Eq. (4.2)

$$\frac{\partial(\ell n \theta)}{\partial z} = \frac{\partial(\ell n T)}{\partial z} - \frac{R}{C_p} \frac{\partial(\ell n P)}{\partial z} \tag{4.2}$$

The hydrostatic equation was substituted into Eqs. (4.1) and (4.2) to give

$$N^2 = \frac{g}{\bar{T}} \frac{\partial T}{\partial z} + \frac{g^2}{T} \frac{1}{C_p} \qquad (4.3)$$

Short gravity waves are removed from the atmosphere by the hydrostatic assumption but the error introduced by this manipulation is small. An order-of-magnitude comparison revealed that the second term on the right-hand side of Eq. (4.3) was one order smaller than the first (typically 10^{-4} compared to 10^{-3}).

Table 7 lists the periods corresponding to the BVF for two layers. One layer extends from 4.57 m to 91.4 m and the second from 30.4 m to 91.4 m. The table shows that the two layers have similar periods with a mean for all cases of 110 sec.

The period corresponding to the low frequencies revealed by the variance spectrum analysis ranged from 7680 sec to 1920 sec. These periods were shorter than the inertial range and longer than the buoyancy oscillation range (BVF). This result suggested that some mechanism at higher levels must be acting to force the observed oscillations.

Two mechanisms have been proposed in recent literature as possible causes of low frequency oscillations. The first is a large-amplitude lee wave as suggested by Danielsen and Bleck (1970) and the second is the hydraulic-jump phenomenon as suggested by Vergeiner (1971).

Table 7

Brunt-Vaisala Periods

Case	4.57-91.4 sec	30.4-91.4 sec
1	108	118
2	110	106
3	86	86
4	92	97
5	112	120
6	88	82
7	87	82
8	130	156
9	115	134
10	109	121
11	107	116
12	123	149
MEAN	106	114

4.4 Amplitudes

At any level on the tower the variance is related to the amplitude by

$$\text{Variance} = \frac{(\text{Amplitude})^2}{2} \qquad (4.4)$$

An estimate of the variance was obtained by averaging the variance values calculated for the sub-segments from each sample. Table 8 shows the mean value and variance for each level on the BBRK tower. Plots of the amplitude as a function of height for each case are shown in Figures 10 to 12. Solid lines represent amplitudes as calculated from the mean variance of the individual blocks. Dashed lines represent amplitudes as calculated from the variance associated with the frequency value at the peak in the spectra at each level.

The amplitude plots can be classified into two groups. The first group, Cases 1, 2, 3, 4, 6, 7, 11, shows the amplitude increasing with height. The second group, Cases 5, 8, 9, 10, 12, shows the amplitude uniform with height or even decreasing at an upper level. Closer examination of Cases 2, 3, 6, 7, 11 revealed that the wave number two was dominant in the spectra at those levels for which the amplitude was greater than 2 C. Usually increased amplitudes were accompanied by a slight shift to higher wave numbers. It was difficult to assess whether this phenomenon was physically real or mathematically induced. The evidence points to the possibility of a real shift in wave number and further investigation would be of interest.

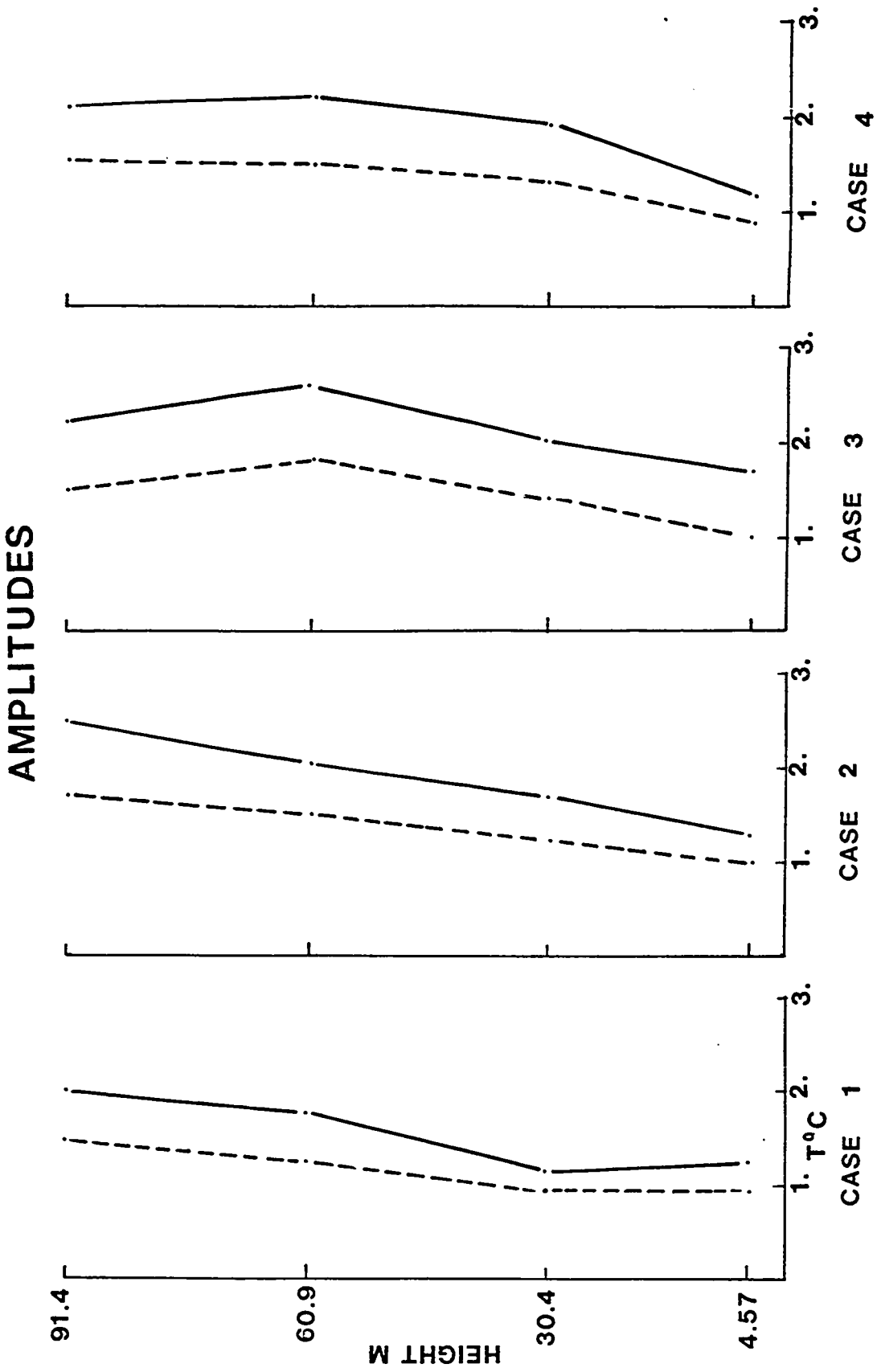

Figure 10. Amplitude (C) versus height (m) from the BBRK tower for Cases 1 to 4.

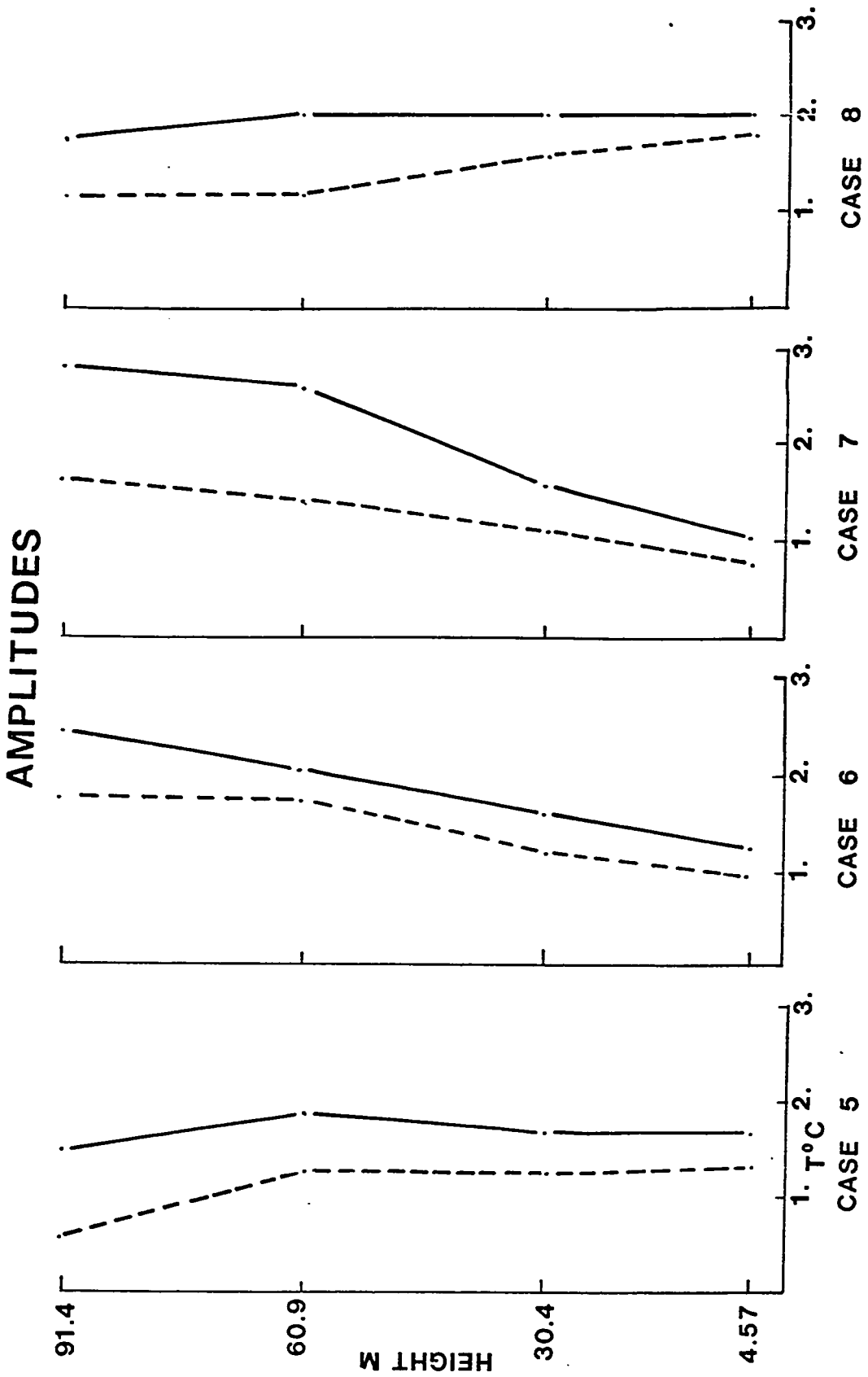

Figure 11. Amplitude (C) versus height (m) from the BBRK tower for Cases 5 to 8.

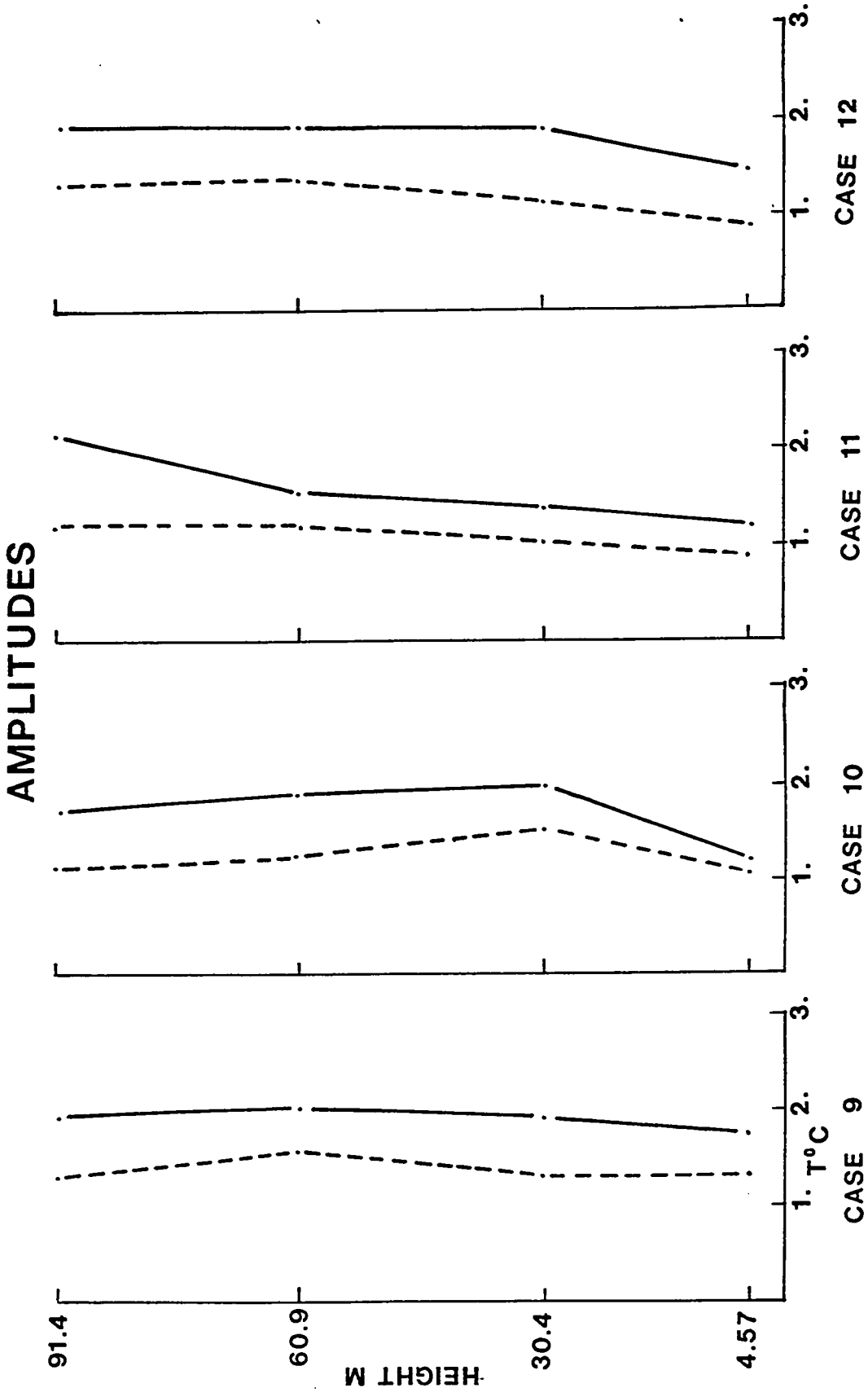

Figure 12. Amplitude (C) versus height (m) from the BBRK tower for Cases 9 to 12.

Table 8

Mean and Variances

	Means C				Variances C^2			
Case	4.57	30.4	60.9	90.4	4.57	30.4	60.9	90.4
1	-8.5	-5.6	-4.1	-1.4	.14	.10	.51	.96
2	-9.2	-7.6	-5.6	-2.4	.14	.48	1.05	2.23
3	-14.1	-10.6	-5.8	-2.4	.46	1.05	2.72	1.46
4	-15	-11.2	-8.6	-4.9	.12	.75	1.50	1.15
5	-10.4	-7.8	-5.4	-3.8	.45	.43	1.85	1.46
6	-20.1	-18.1	-13.9	-9.3	.11	.38	1.07	2.21
7	-14.7	-12.6	-8.4	-3.4	.07	.33	7.52	3.62
8	-8.9	-6.3	-4.9	-4.2	.99	.99	.98	.22
9	-1.9	1.3	2.6	4.5	.58	.78	.95	.78
10	-5.9	-2.9	-0.9	1.1	.10	.85	.73	.47
11	-17.0	-14.1	-12.8	-9.9	.11	.21	.31	.62
12	-3.5	-0.5	0.5	1.94	.24	.76	.77	.81

4.5 Temperature Gradient, Shear and Richardson Number

Figure 5 from Holmes and Hage (1971) showed that the warm air penetration to the surface was accompanied or preceded by an increase in the mean vertical shear of the horizontal wind and a decrease in the mean vertical temperature gradient. Calculations of Richardson number (Ri) sequences at times relative to the inversion breakdown were considered to be of importance. Ri as defined in Lumley and Panofsky (1964) is

$$Ri = N^2 \Big/ \left(\frac{\partial u}{\partial z}\right)^2 \qquad (4.5)$$

Figures 13 to 15 show the shear in units of m sec^{-1} $(100\ m)^{-1}$, temperature gradient in C $(100\ m)^{-1}$, and Ri for three cases. Points at which the winds at the top and bottom levels of BBRK were reported calm are plotted with a small circle. The Ri is undefined in the limit as $(\partial u/\partial z)$ approaches zero.

The denominator in Eq. (4.5) was calculated assuming a linear profile throughout the 91 m tower. Values of temperature and wind used in Eq. (4.5) were averaged over 30 min ± 15 min. on the mid points of the subsegments for each sample.

Calculations were performed for three cases and the following observations were made:

(i) the plots of temperature gradient and vertical shear of the horizontal wind reflected the average shape found by Holmes and Hage (1971). There was, however, a scatter among the individual samples. The shear increased before or during the inversion breakdown.

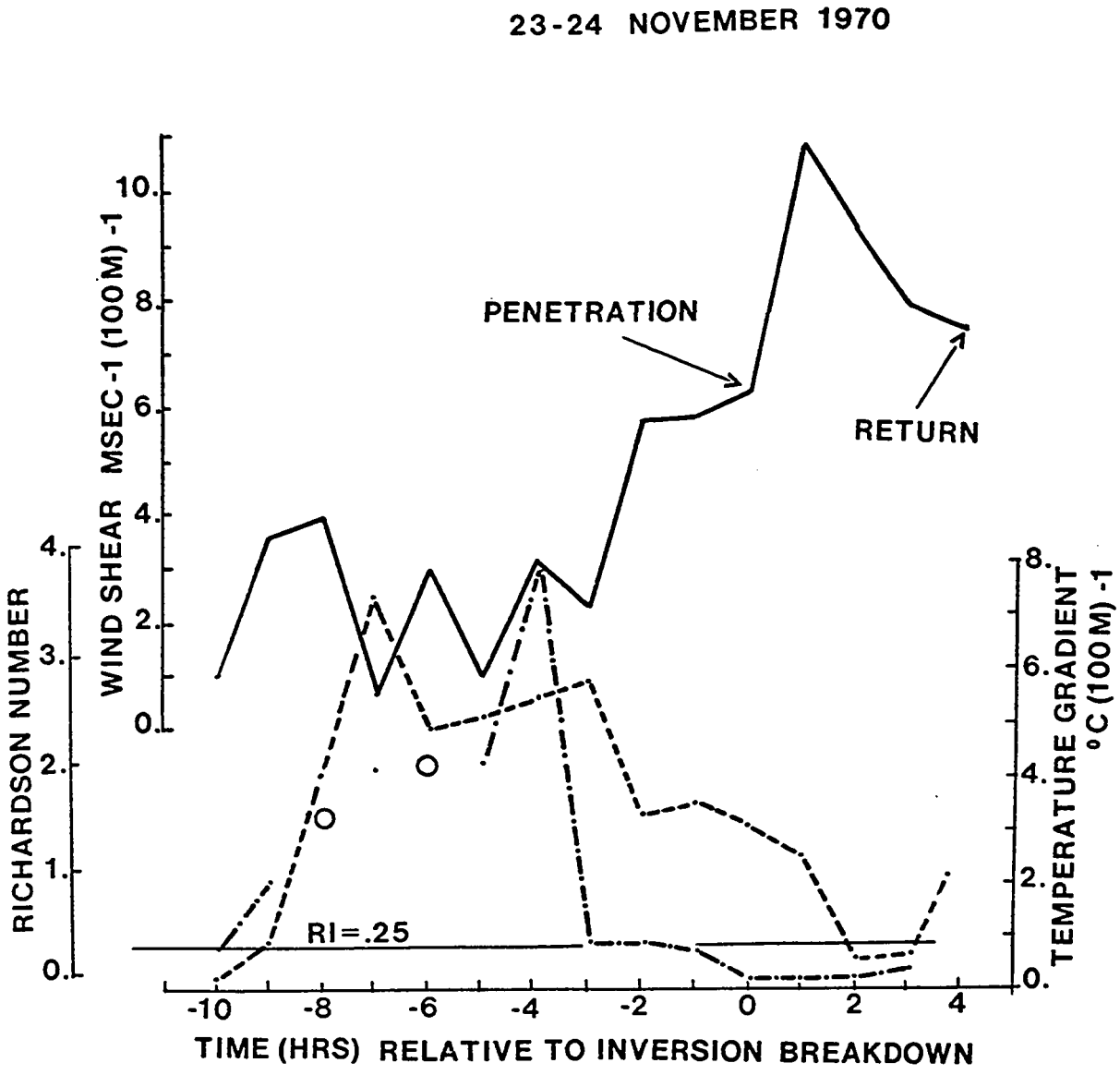

Figure 13. Values of the vertical shear of the horizontal wind speed, vertical temperature gradient and Richardson Number for Case 2.

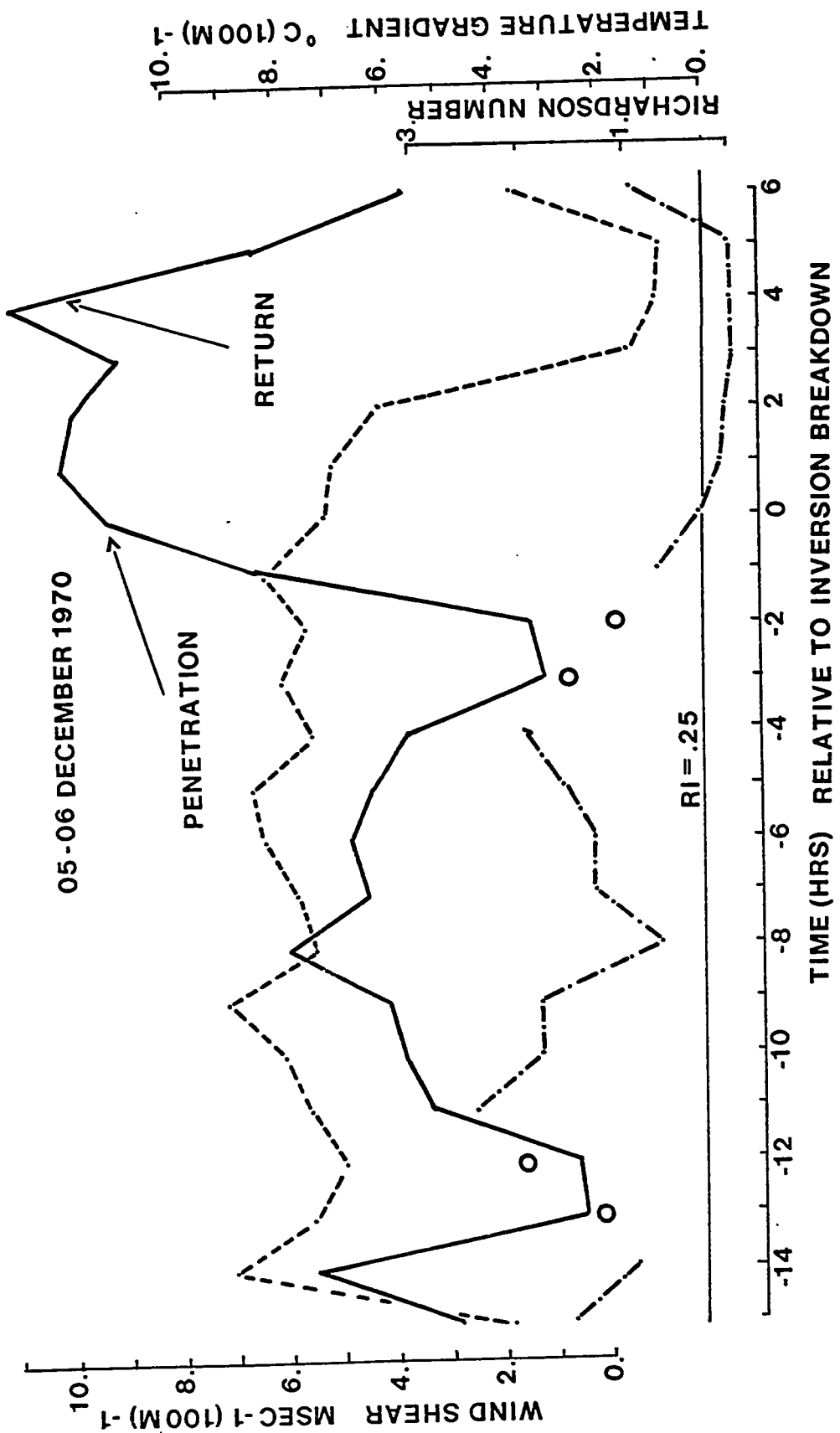

Figure 14. Values of the vertical shear of the horizontal wind speed, vertical temperature gradient and Richardson Number for Case 3.

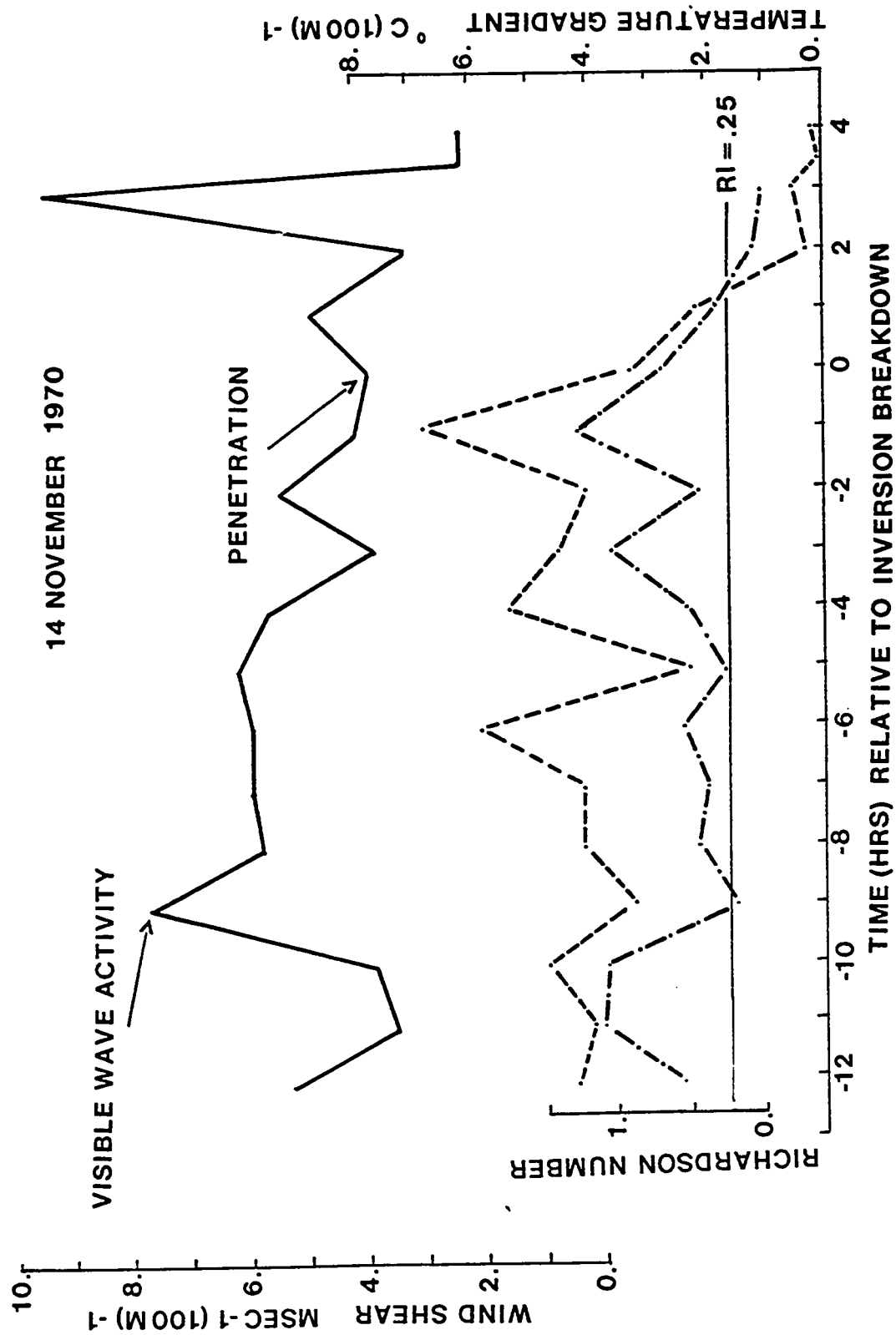

Figure 15. Values of the vertical shear of the horizontal wind speed, vertical temperature gradient and Richardson Number for Case 1. A portion of the data sample in which the temperature fluctuations were well organized is marked (visible wave activity).

(ii) an unexplained smaller decrease in the shear preceded the larger increase associated with the inversion breakdown.

(iii) Ri decreased gradually from positive values greater than +0.25 to less than +0.25 during the inversion breakdown. A critical value of Ri = +0.25 has been postulated for the transition from laminar to turbulent flow (Taylor, 1931).

The assumption of a linear wind profile in stable air needed for the calculation of the denominator in Eq. (4.5) is an over-simplification of the wind structure in a stable atmosphere. However, according to Lumley and Panofsky (1964) no simple wind profile formula is known for stable air. The linear assumption may be the best available under the circumstances.

The evidence suggests, although not conclusively, that the penetration of warm air to the surface occurred under conditions favourable for the release of shearing instability.

4.6 Temporal Distribution of Variance

The variances as calculated for each segment of a sample were plotted as a function of time using the mid-point of each segment. Two such plots are presented in Figures 16 and 17. Graphing the variance in this way represents a time sequence of variance relative to the inversion breakdown because the blocks are numbered relative to the inversion breakdown.

The variance exhibited a degree of periodicity, particularly the 60.4 m level on 5-6 December 1970 (Figure 17). The variance increased to a peak at -14 followed by a decrease and then increasing

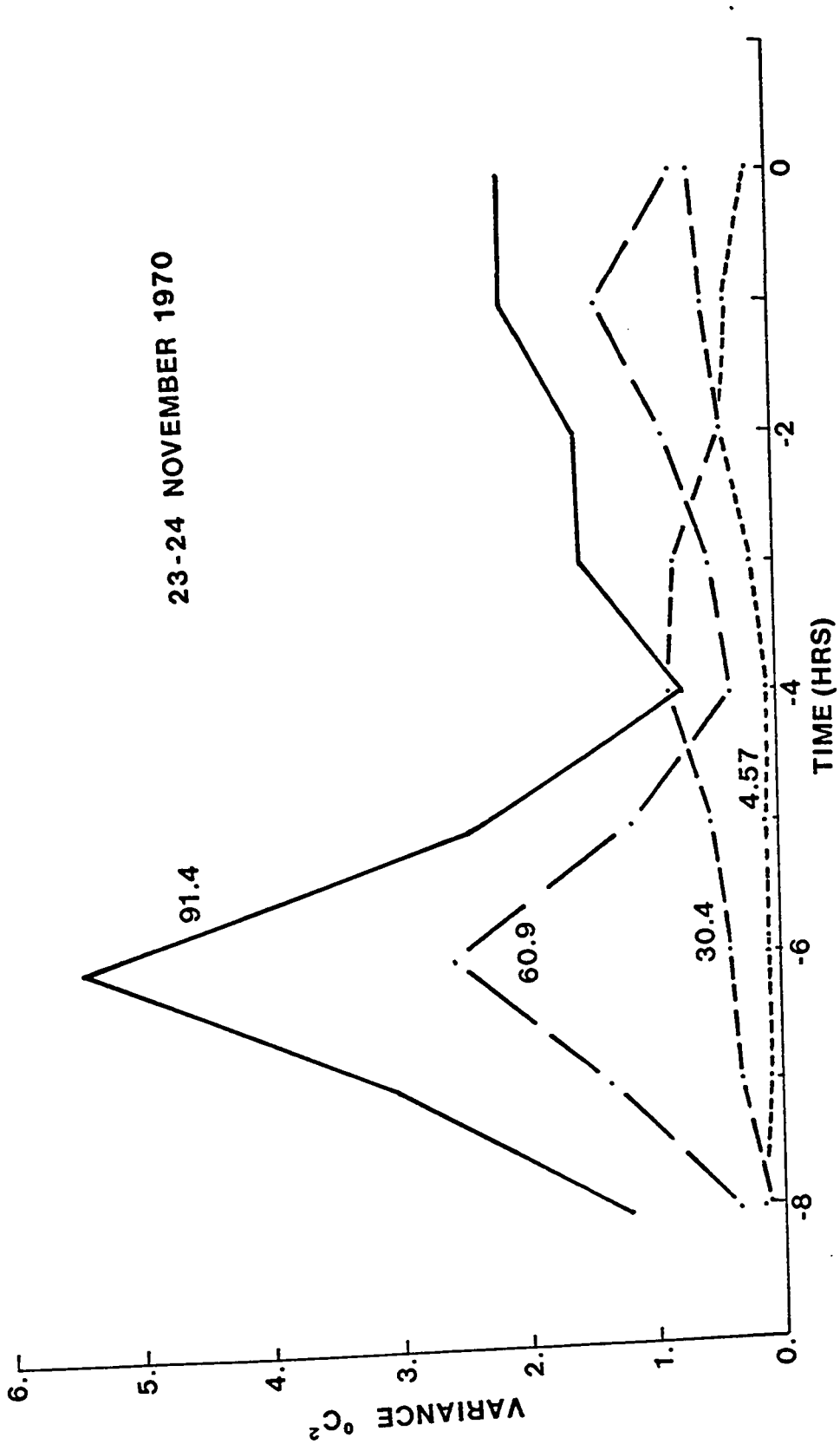

Figure 16. Variance of the temperature versus time (HRS) relative to the inversion breakdown.

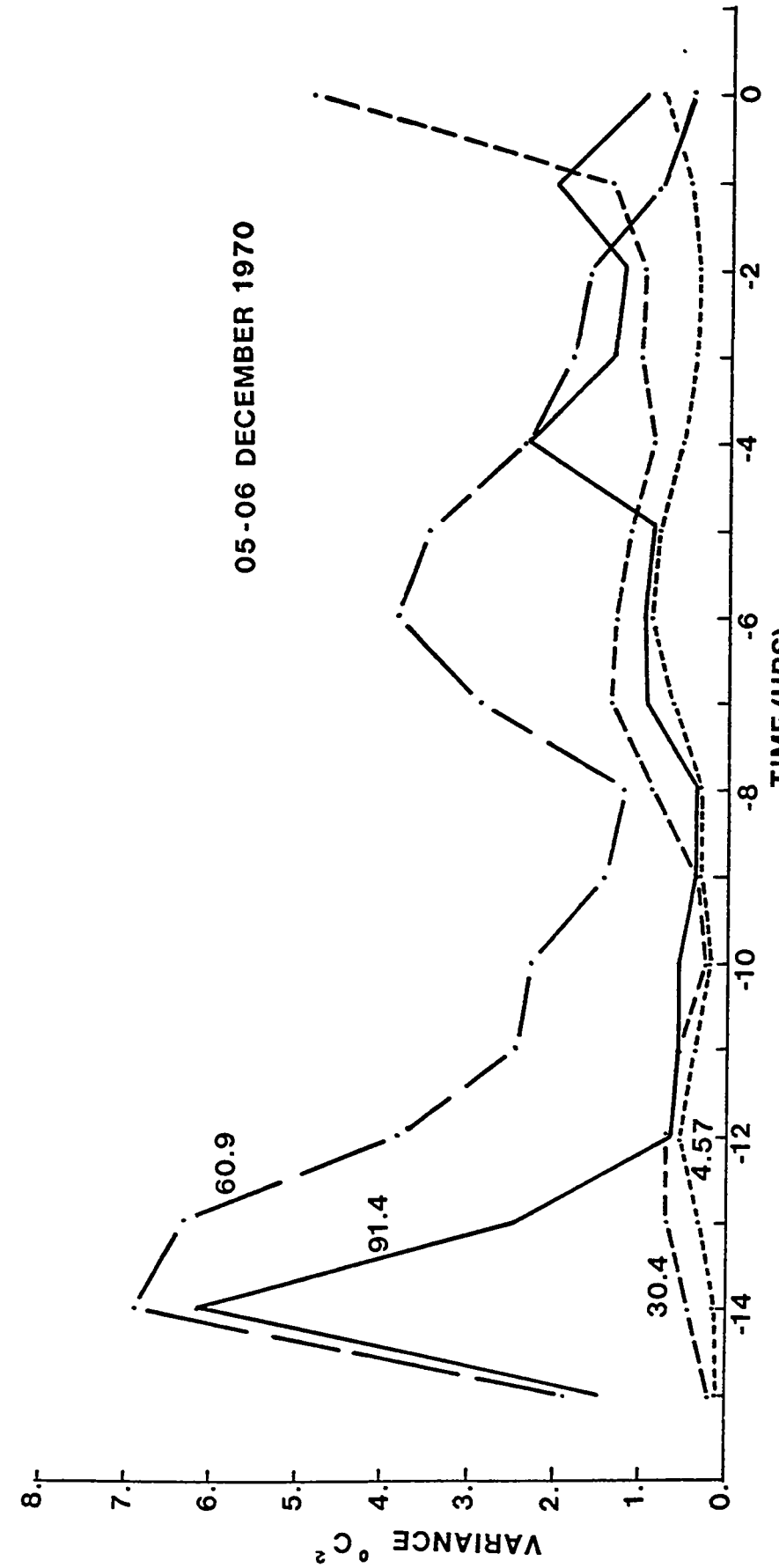

Figure 17. Variance of the temperature versus time (HRS) relative to the inversion breakdown.

to a peak at -6. This interval of eight hours was appreciably longer than the periods investigated previously by means of spectral analysis. The evidence suggests that a long period oscillation may have produced the shear necessary to cause the shorter waves to break. Hallett (1972) suggested that the breaking mechanism itself destroys the situation that produces it and that a stable longer wave may be the initiating mechanism. Whether or not the oscillations described here have all the properties of true waves cannot be established because of data limitations.

4.7 Slope of Penetration

The rate of warm-air penetration was estimated from the slope of the observed inversion breakdown.

Table 9 lists the rates of warm-air penetration in units of F min^{-1}. Calculations were performed using the data records by dividing the temperature change by the time required for the change to occur. The steep slopes of Cases 2 and 3 were associated with the largest values and longest durations of shear as shown in Figures 13, 14, and 15.

4.8 Spatial Distribution

The spatial distribution of the warm-air penetration to the surface was considered to be one of the most interesting aspects to be explored.

Unfortunately the quality of the data was such as to make conclusions unreliable. The thermograph records from the fire halls

Table 9

Rates of Warm-Air Penetration (F min^{-1})

Case	4.57 m	30.4 m	60.9 m	91.4 m
1	.14	.08	.06	.02
2	.36	.33	.29	.22
3	.28	.25	.14	.07

recorded the main features of the surface warming, but the time scale was too coarse to resolve time differences between the various stations. The surface warming did occur at all of these stations throughout Calgary. At the chinook research stations the data showed the main features of the surface warming, but again accurate time resolution between stations was not possible. An accurate log of time and temperature corrections was unavailable. The CFCN tower data recorded at the western outskirts of Calgary provided confirmation of some of the details recorded on the BBRK tower. Regretfully, however, an accurate time log was not kept for these data.

An estimate of cross covariance between the 91 m level on the BBRK tower and the 35 m level on the CFCN tower was calculated. Mean lagged products were calculated for every tenth point of the BBRK data. This adjustment was necessary because the sampling frequency on the BBRK tower was ten times that of the CFCN tower.

The cross covariance showed a maximum at a positive lag

of 13 min. This calculated lag confirmed a lag of 12 min estimated visually by overlaying plots of the events from the two towers.

Using a separation of 11.9 km between the towers the phase speed was estimated by

$$c = \frac{\Delta s}{\Delta t} \tag{4.6}$$

where Δs is the distance separation and Δt the time lag. The calculated phase speed was 15.3 m sec^{-1}. Assuming G. I. Taylor's (1938) hypothesis, (see Lumley and Panofsky, 1964), the wavelength λ can be found from

$$\lambda = c\tau \tag{4.7}$$

where τ is the period. Equation (4.7) yields a wavelength in the range of 29 to 118 km. This range encompasses the wavelength values identified by Holmes and Hage (1971).

The significance of this result cannot be judged categorically because of the limitations imposed by the data.

CHAPTER V

SUMMARY AND CONCLUSIONS

South-west Alberta is well known for the intensity of inversions that develop in winter with air aloft that has been warmed by subsidence over the mountains and cold air below associated with stagnant lee anticyclones. Frequently in the course of each winter the warm air penetrates to the surface and Foehn (chinook) conditions prevail.

Continuous recordings of temperature and wind at several levels on a 91 m tower within the city of Calgary in the period 1968-1972 provided an unusual opportunity to study lower atmospheric changes prior to and during the onset of the chinook.

Visual examination of tower temperature records prior to the onset of chinooks showed that (a) large temperature oscillations (up to 2.5 C in amplitude) were common at the 91 m and 61 m levels for many hours prior to surface warming and (b) the chinook was preceded by a gradual increase in intensity of the inversion (up to 9 C/100 m) followed by a sudden breakdown (11 to 75 min) and the establishment of near isothermal temperature gradients in the lowest 100 m.

Twelve cases that exhibited these features and that ranged in length from 4-18 hours were selected for detailed analysis. An examination of concurrent upper air soundings and upper air charts revealed that all cases occurred in strong westerly flows aloft (12-32 m sec^{-1} at 500 mb) and in air that was statically stable to great heights.

Variance spectra and cross-spectra (between levels) were computed for the selected samples of temperature data. These spectra covered the frequency range from 1 cycle in 128 min to 64 cycles in 128 min. The spectra and cross-spectra exhibited significant maxima in frequencies 1 cycle in 128 min to 4 cycles in 128 min (periods of 7680 sec to 1920 sec). These fall between characteristic Brunt-Vaisala and inertial frequencies. This evidence resulted in the conclusion that some other atmospheric phenomenon, possibly a hydraulic-jump or a large amplitude lee wave, was acting to force the observed oscillations.

The amplitude of the temperature oscillation increased with height on the tower in most cases. However, in some the amplitude remained essentially constant with height. No significant phase lags between tower levels could be found.

Calculated values of the vertical shear of the horizontal wind and the vertical temperature gradient were in good agreement with mean values computed by Holmes and Hage (1971). The Richardson number decreased below the critical value of +0.25 during the inversion breakdown. It was concluded that shearing instability (Kelvin-Helmholtz) may have been responsible for the inversion

breakdown and represented a possible source of low level turbulence.

The time changes in temperature variance pointed to the possible existence of a longer primary wave that might have controlled initiation of the inversion breakdown.

The rate of warm air penetration to the surface was estimated from the slope of the observed temperature with time from the data samples during inversion breakdown. The steeper slope (faster rate of penetration) was associated with stronger vertical shear of the horizontal wind.

Regretfully, inadequacies in the available data placed limitations on the significance of conclusions drawn concerning the spatial distribution of these phenomena.

Rapid surface warming was recorded at the Chinook Research Stations as far out as 63 km from the city of Calgary. Within the city, the onset of surface warming was shown by a set of thermographs situated throughout the city. Large amplitude temperature fluctuations were recorded at both towers on the west and southeast sides of Calgary.

The length of the waves acting during these events was roughly estimated to range from 25 to 130 km.

BIBLIOGRAPHY

BIBLIOGRAPHY

Bendat, J. S., and A. G. Piersol, 1966: Measurement and Analysis of Random Data. New York, Wiley & Sons, 390 pp.

Bingham, C., M. D. Godfrey and J. W. Tukey, 1967: Modern Techniques of Power Spectrum Estimation. IEEE Transactions on Audio and Electroacoustics, AU-15, 56-66.

Blackman, R. B. and J. W. Tukey, 1958: The Measurement of Power Spectra. New York, Dover Publications, 190 pp.

Cochran, W. T., J. W. Cooley, D. L. Favin, H. D. Helms, R. A. Kaenel, W. W. Lang, G. C. Maling, Jr., D. E. Nelson, C. M. Rader, and P. D. Welch, 1967: What is the fast Fourier transform? IEEE Transactions on Audio and Electroacoustics, AU-15, 45-55.

Cooley, J. W., P. A. W. Lewis, and P. D. Welch, 1969: The Application of the fast Fourier Transform Algorithim to the Estimation of Spectra and Cross Spectra. Proc. Symp. on Computer Processing in Communications, 19, 5-20.

Danielson, E. F. and R. Bleck, 1970: Tropospheric and Stratospheric Ducting of Stationary Mountain Lee Waves. J. Atmos. Sci., 27, 758-772.

Eddy, A., C. E. Duchon and J. A. Almazan, 1968: Variance Spectrum Analysis. Atmospheric Science Group, University of Texas Report No. 8, 356 pp.

Fisher, Sir R. A., 1958: Statistical Methods for Research Workers. Edinburgh, Oliver and Boyd, 13th ed., 296 pp.

Förchtgott, J., 1950: The Transport of Small Particles or Insects Over the Öre Mountains. Bull. Met. Czech., Prague, 4, 14-16.

Glenn, C. L., 1961: The Chinook. Weatherwise, 14, 175-182.

Hallett, J., 1972: Breaking Waves at an Inversion. Mon. Wea. Rev., 100, 133-135.

Holmes, R. M. and K. D. Hage, 1971: Airborne Observations of Three Chinook-Type Situations in Southern Alberta. J. Appl. Meteor., 10, 1138-1153.

Jenkins, G. M., 1961: General Considerations in the Analysis of Spectra. Technometrics, 3, 133-166.

Kellie, A. R., 1972: Practical Considerations for Variance Spectrum Analysis. University of Alberta, Computing Review, 5, 48-62.

Kuettner, J. and C. F. Jenkins, 1953: Flight Aspects of the Mountain Wave. Air Force Cambridge Research Center, Surveys in Geophysics, Tech. Report No. 35., 37 pp.

Lilly, D. K., 1967: Techniques for the Study of Mountain Waves. Facility for Atmospheric Research (NCAR) No. 4., 12-16.

Lilly, D. K., 1972: Wave Momentum Flux - A Garp Problem. Bull. Amer. Meteor. Soc., 51, 17-23.

Longley, R. W., 1967: The Frequency of Winter Chinooks in Alberta. Atmosphere, 5, 4-16.

Lumley, J. L. and H. A. Panofsky, 1964: The Structure of Atmospheric Turbulence. New York, Wiley & Sons, 239 pp.

Marsh, J. S., 1965: The Chinook and its Geographical Significance in Southern Alberta. Unpublished M.Sc. Thesis, Department of Geography, University of Calgary, 121 pp

Queney, P., G. A. Corby, N. Gerbier, H. Koschmieder, and J. Zurep, 1960: The Airflow over Mountains. W.M.O. Tech. Note No. 34, 135 pp.

Sawyer, J. S., 1956: The Physical and Dynamical Problems of Orographic Rain. Weather, 11, 375-381.

Scorer, R. S., 1949: Theory of Waves in the Lee of Mountains. Quart. J. Roy. Meteor. Soc., 75, 41-57.

Schuster, A., 1900: The Periodogram of Magnetic Declination. Trans. Camb. Phil. Soc., 109-135.

Starr, J. R. and K. A. Browning, 1972: Observations of Lee Waves by High-Power Radar. Quart. J. Roy. Meteor. Soc., 98, 73-85.

Steenbergen, J. D., 1971: Comparison of Urban and Rural Turbulence Statistics at Edmonton, Alberta. Unpublished M.Sc. Thesis, Dept. of Geography, University of Alberta, 86 pp.

Suzuki, S. and K. Yabuki, 1956: The Airflow Crossing over the Mountain Range. Geophys. Mag., Tokyo, 27, 273-291.

Taylor, G. I., 1931: Effects of Variation in Density on the Stability of Superposed Streams of Fluid. Proc. Roy. Soc., A132, 499-523.

_____, 1938: The Spectrum of Turbulence. Proc. Roy. Soc., A164, 476-490.

Vergeiner, I., 1971: An Operational Linear Lee Wave Model for Arbitrary Basic Flow and Two-Dimensional Topography. Quart. J. Roy. Meteor. Soc. 97, 30-59.

_____, and D. K. Lilly, 1970: The Dynamic Structure of Lee Wave Flow as Obtained from Balloon and Airplane Observations. Mon. Wea. Rev., 98, 220-232.

Welch, P. D., 1967: The Use of the Fast Fourier Transform for the Estimation of Power Spectra: A Method Based on Time Averaging Over Short, Modified, Periodograms. IEEE Transactions on Audio and Electroacoustics, AU-15, 70-73.

APPENDIX

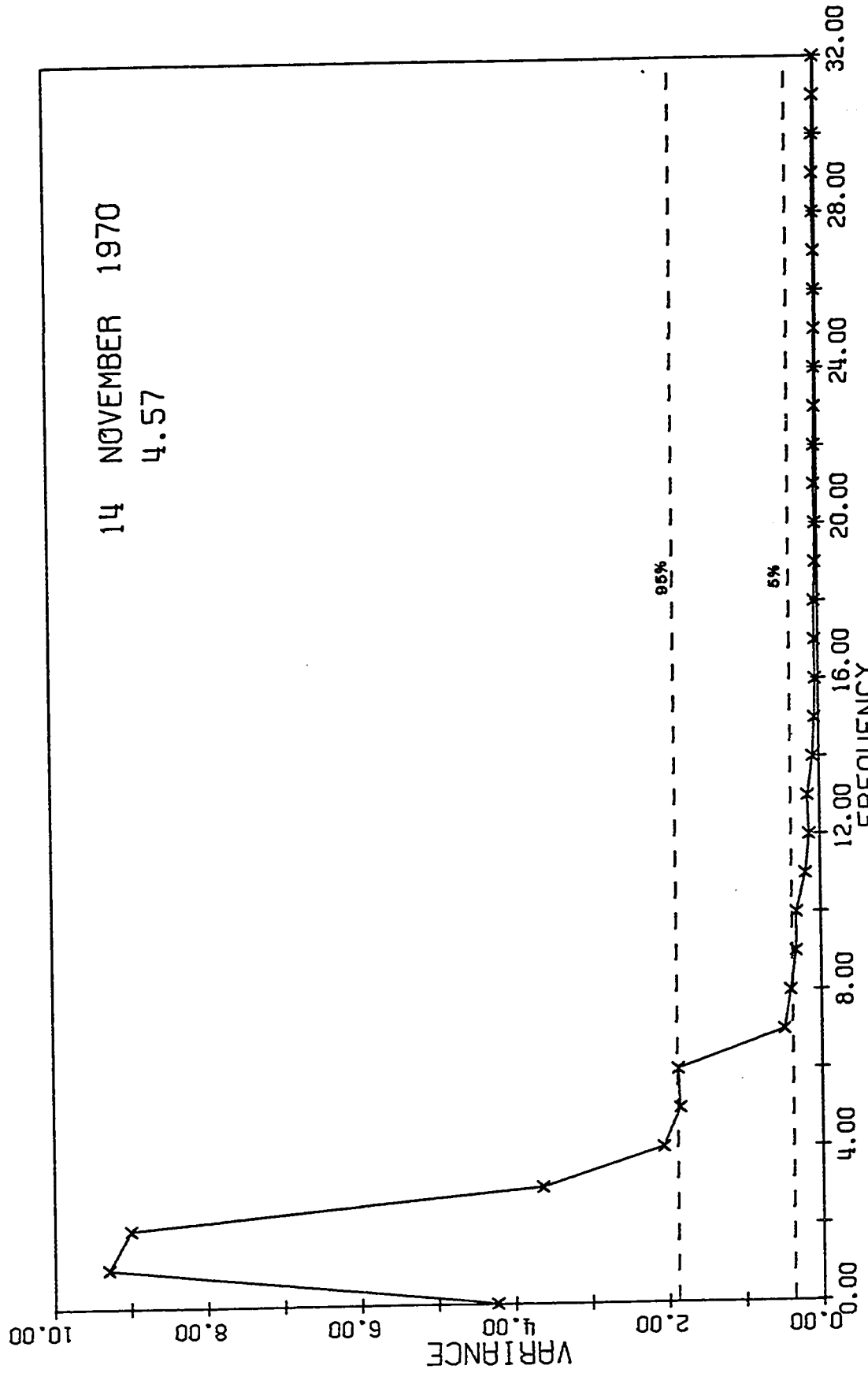

Figure A-1. Variance spectrum of temperature. Normalized variance versus frequency (cycles per 128 min.).

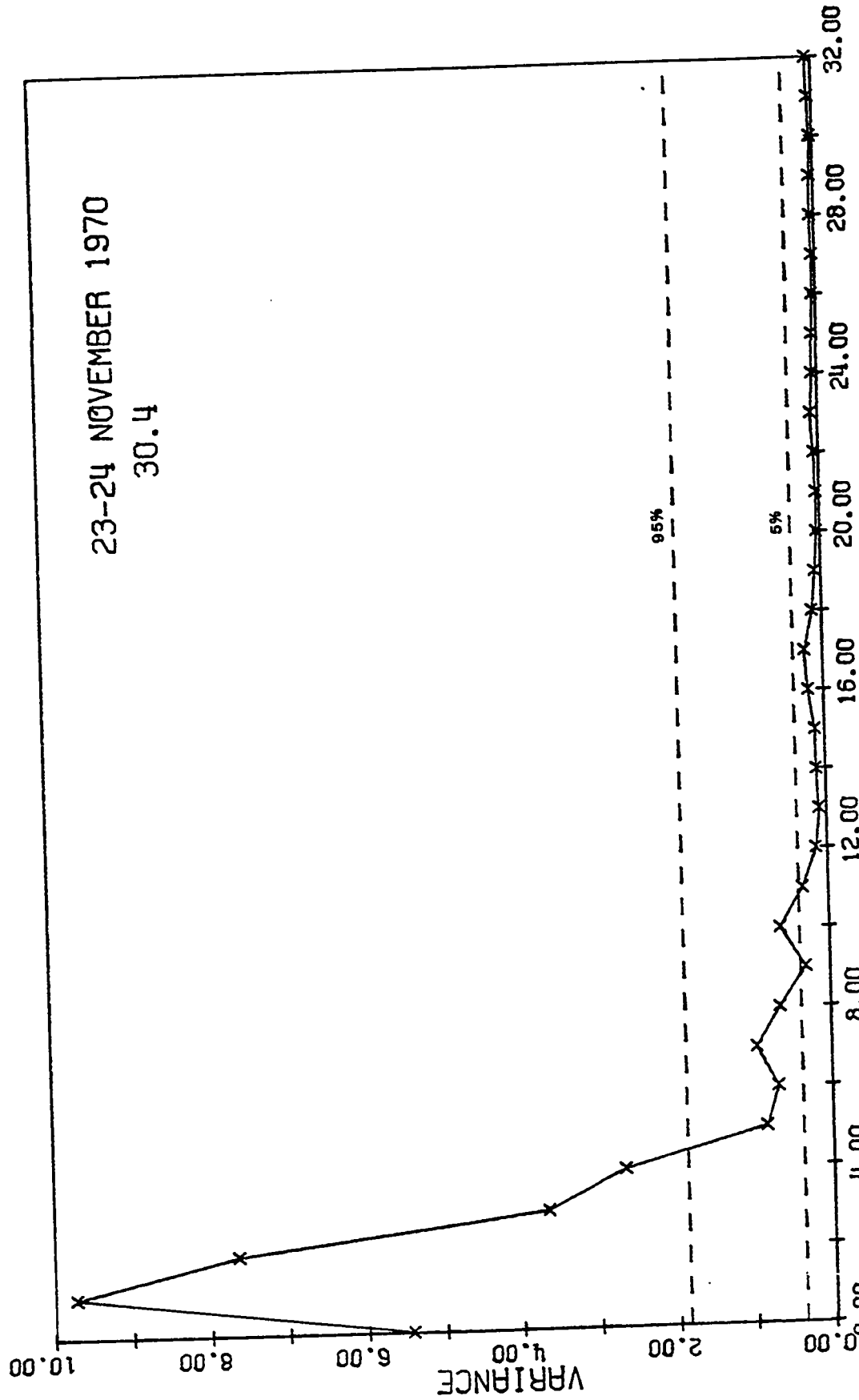

Figure A-2. Variance spectrum of temperature. Normalized variance versus frequency (cycles per 128 min.).

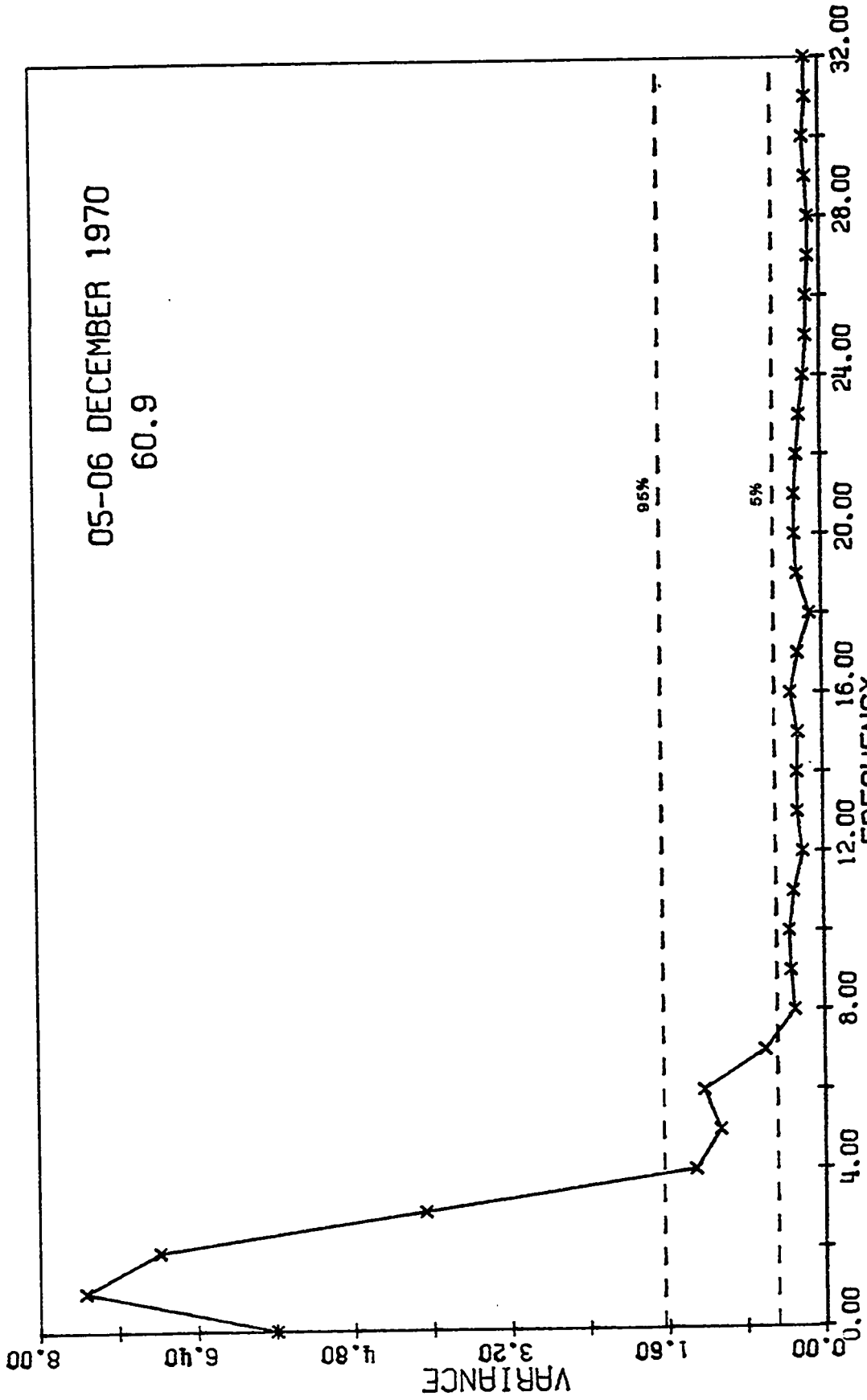

Figure A-3. Variance spectrum of temperature. Normalized variance versus frequency (cycles per 128 min.).

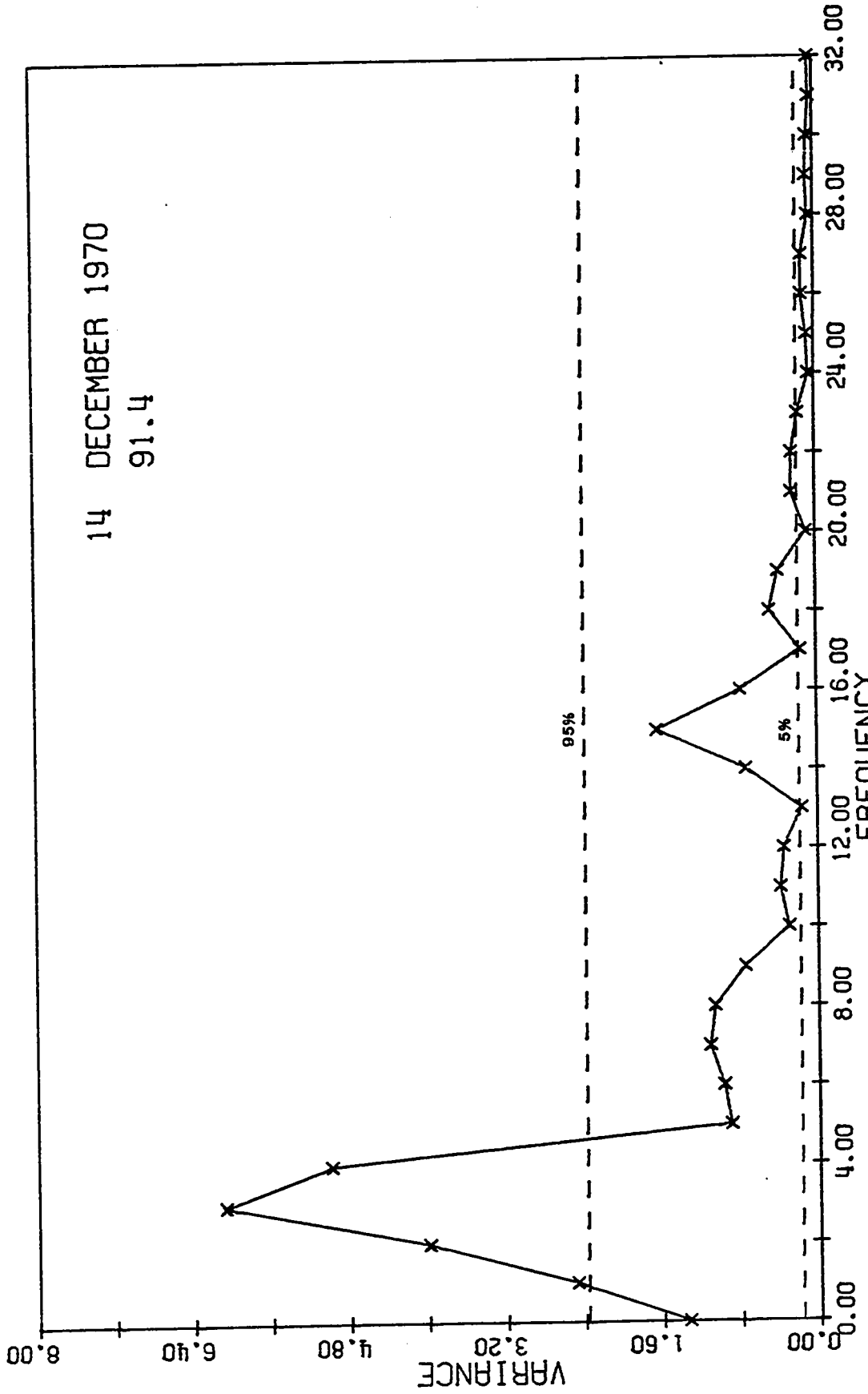

Figure A-4. Variance spectrum of temperature. Normalized variance verzus frequency (cycles per 128 min.).

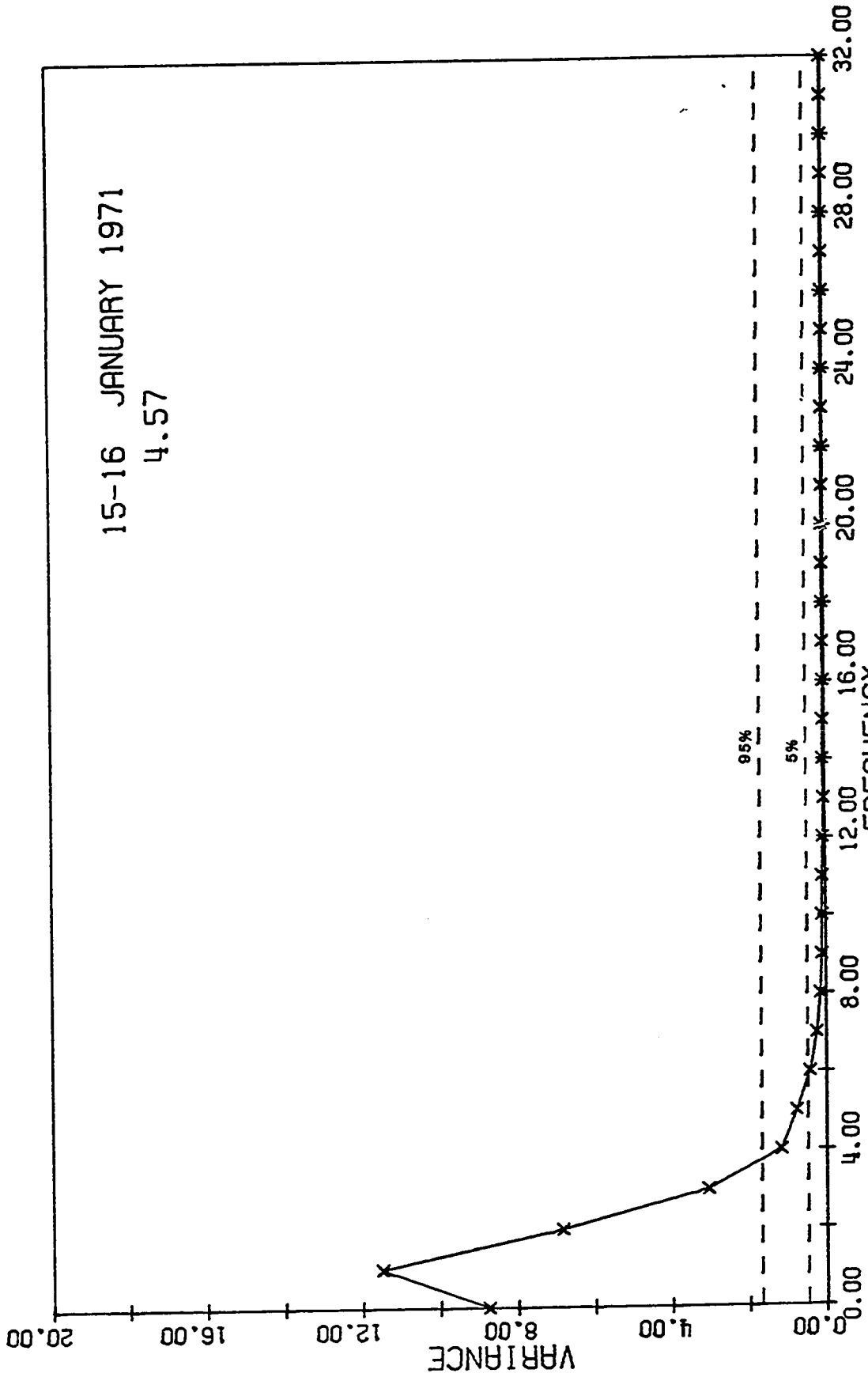

Figure A-5. Variance spectrum of temperature. Normalized variance versus frequency (cycles per 128 min.).

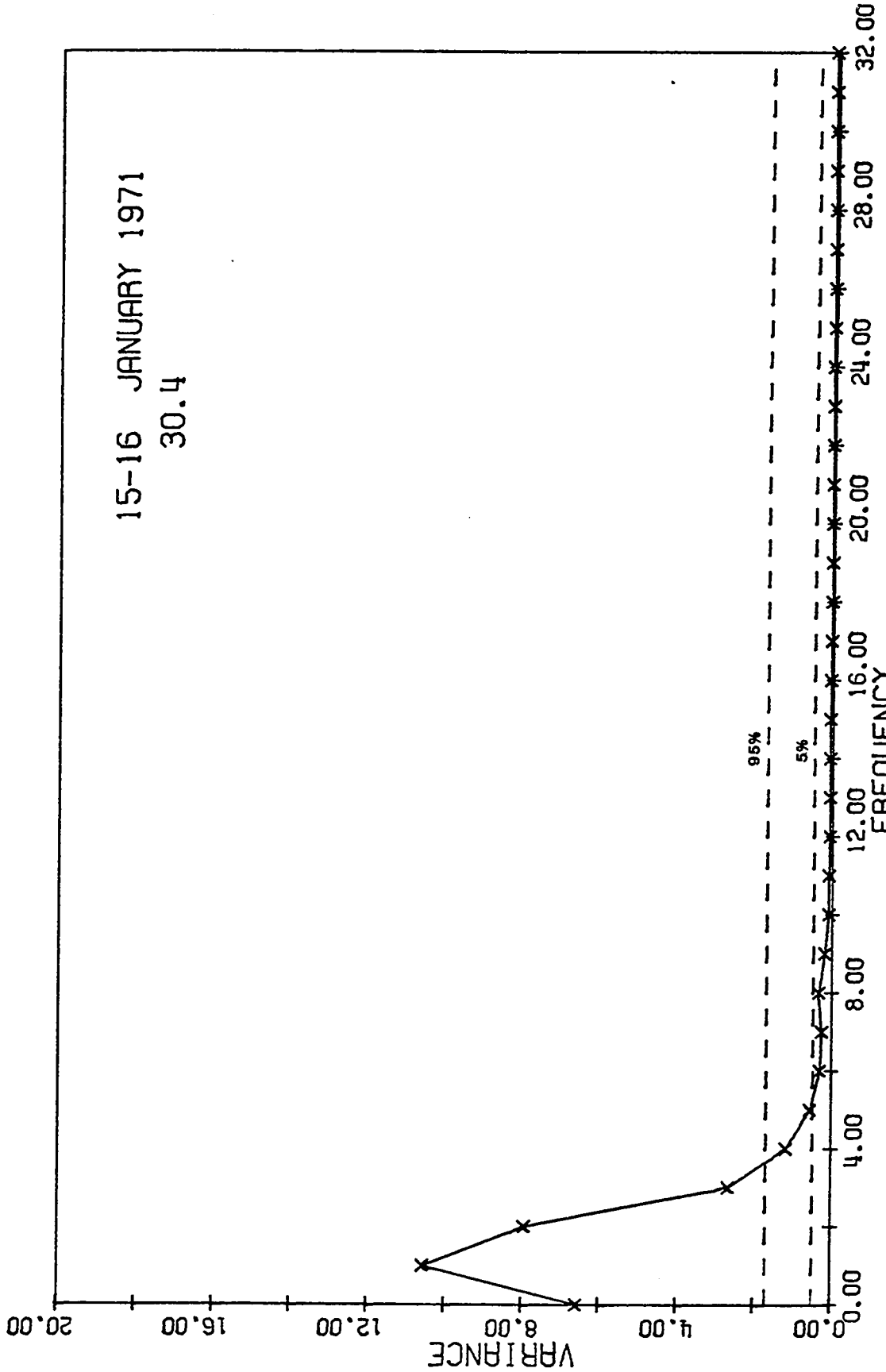

Figure A-6. Variance spectrum of temperature. Normalized variance versus frequency (cycles per 128 min.).

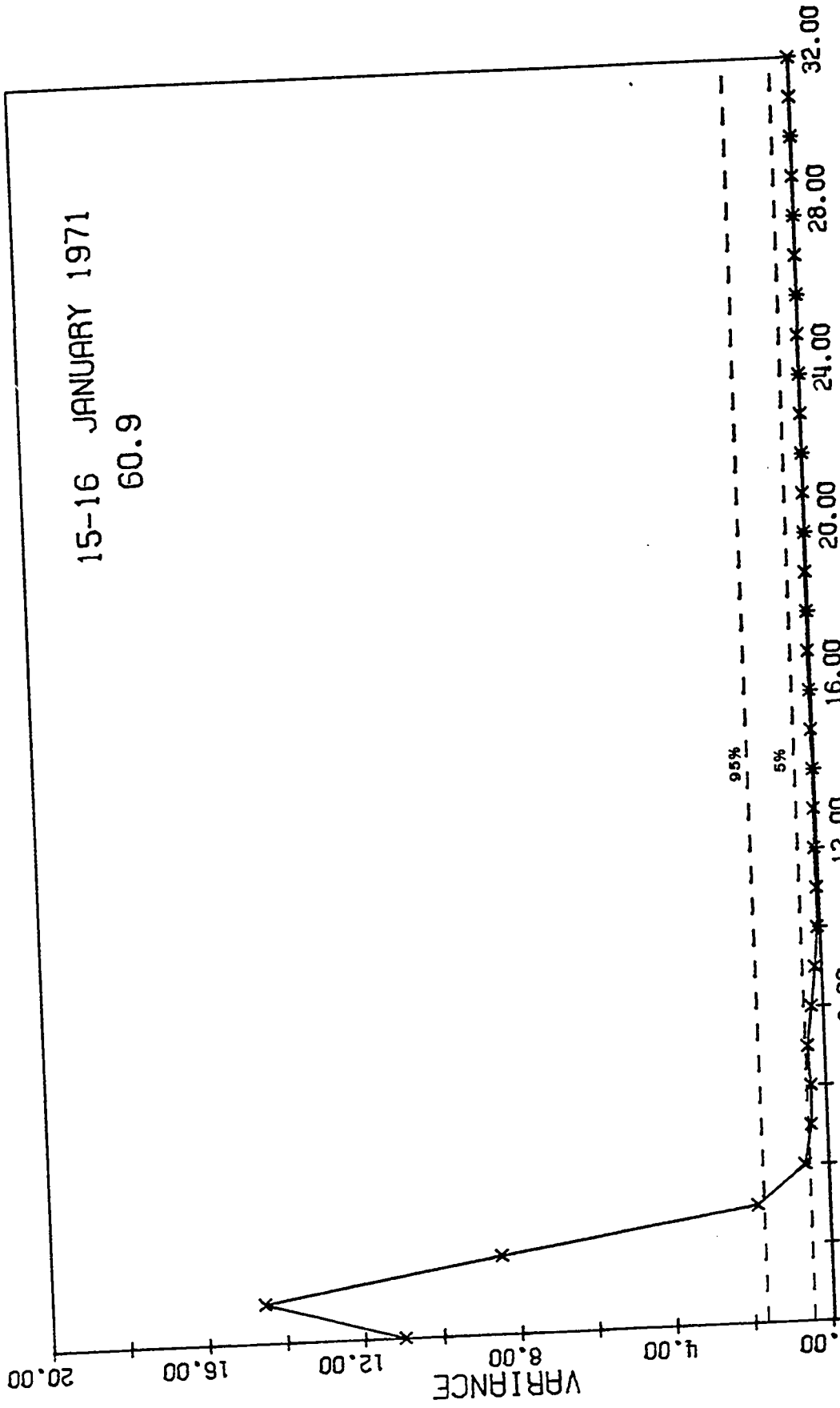

Figure A-7. Variance spectrum of temperature. Normalized variance versus frequency (cycles per 128 min.).

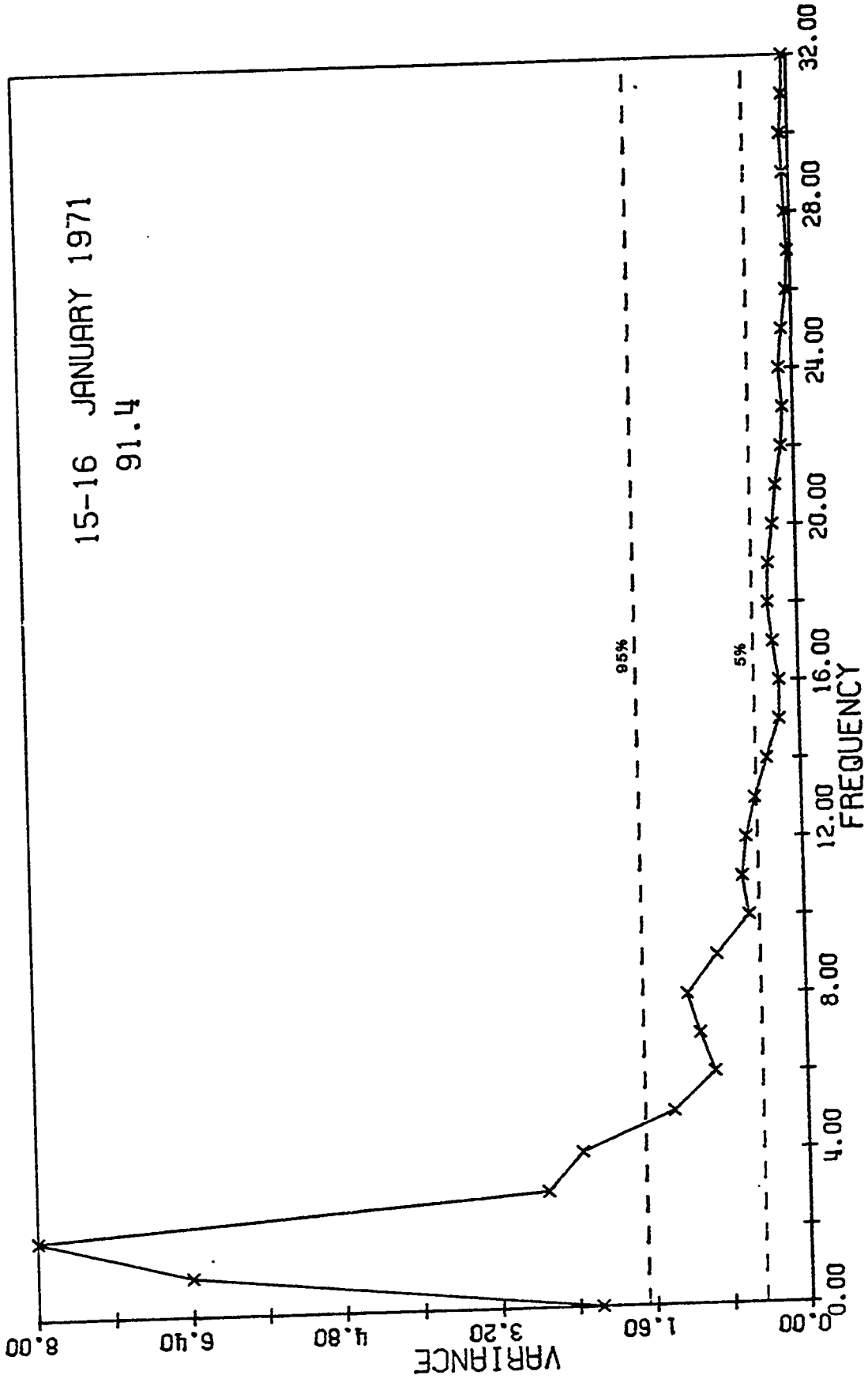

Figure A-8. Variance spectrum of temperature. Normalized variance versus frequency (cycles per 128 min.).

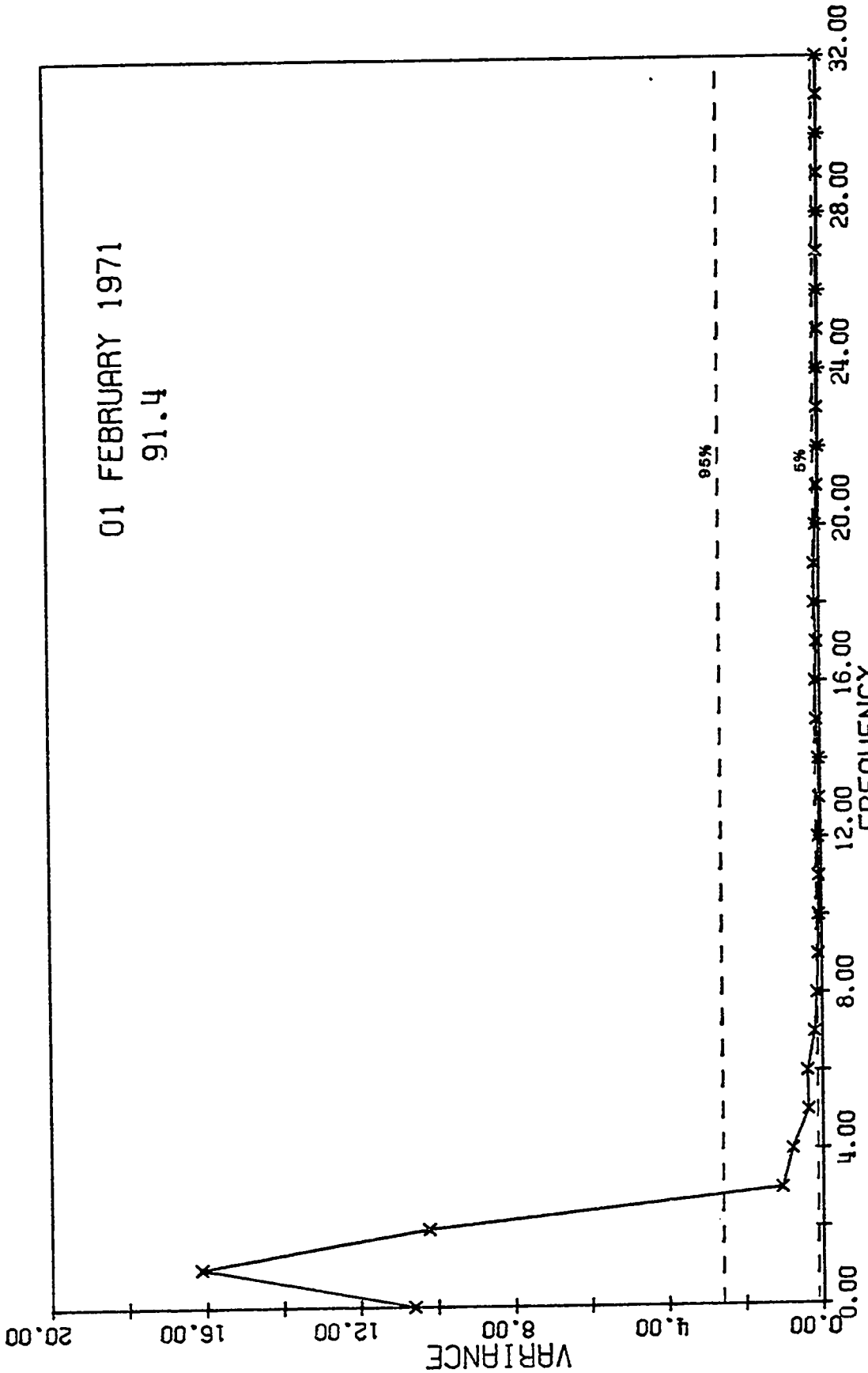

Figure A-9. Variance spectrum of temperature. Normalized variance versus frequency (cycles per 128 min.).

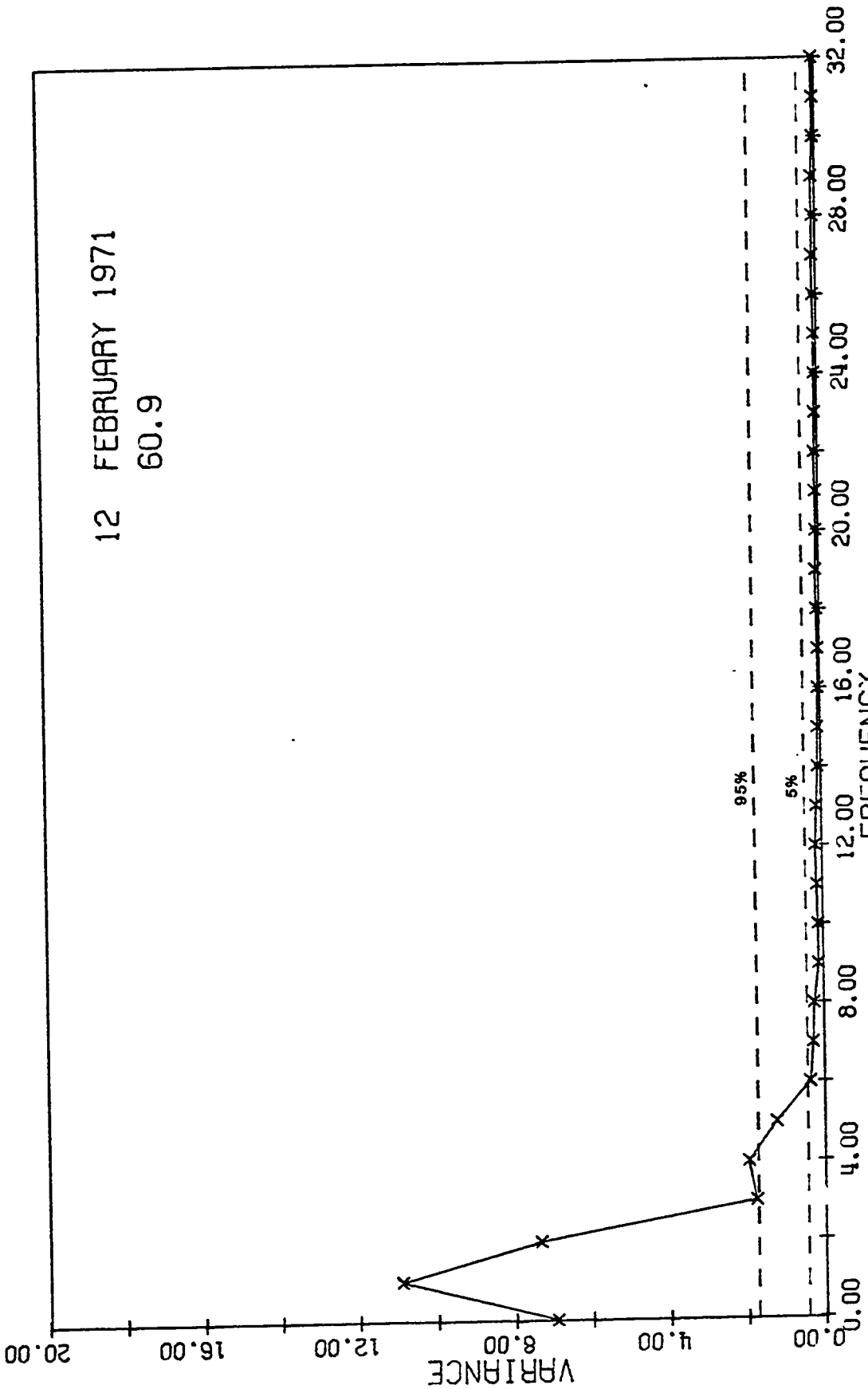

Figure A-10. Variance spectrum of temperature. Normalized variance versus frequency (cycles per 128 min.).

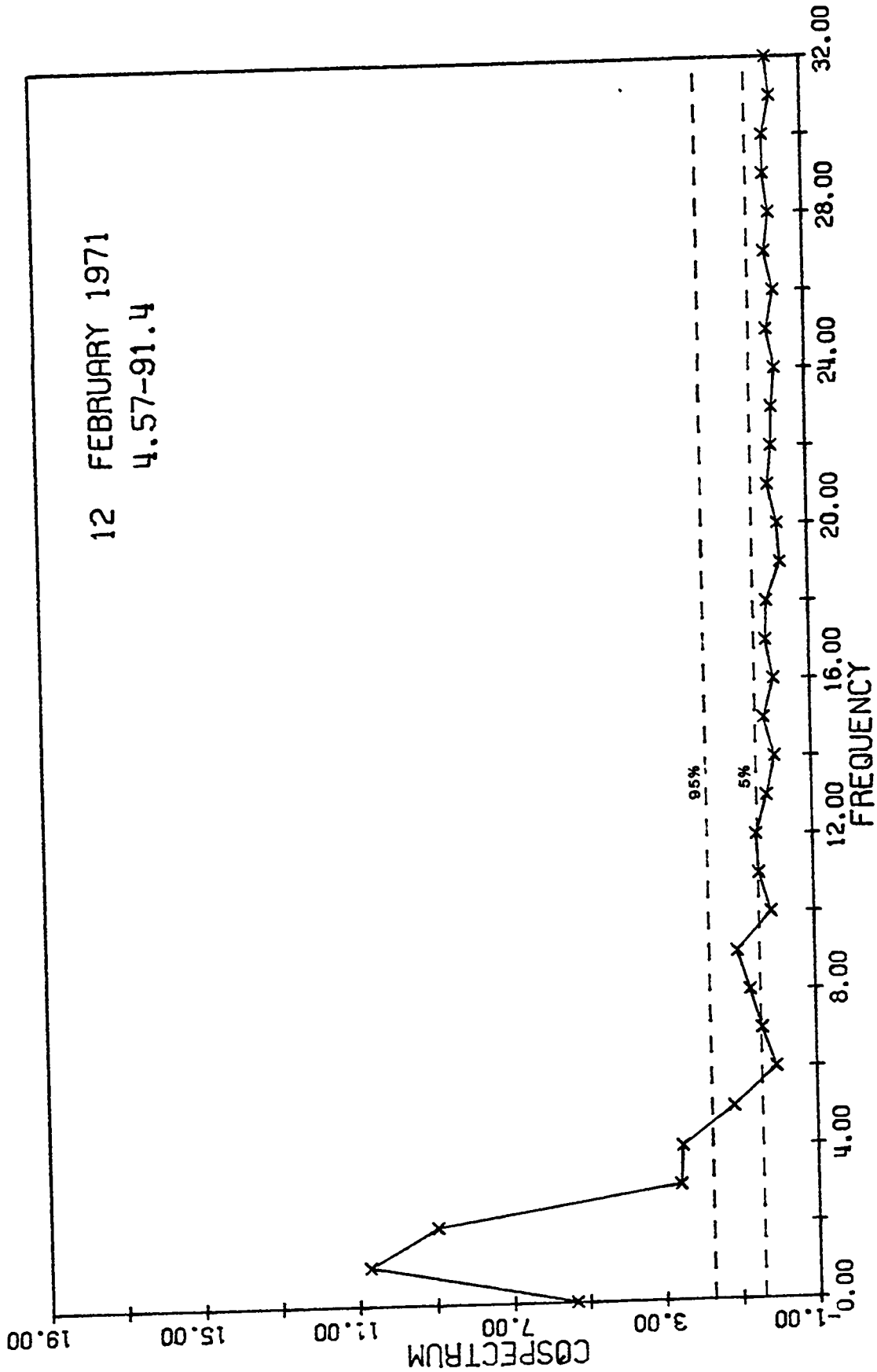

Figure A-11. Cospectrum of temperature. Normalized cospectrum versus frequency (cycles per 128 min.).

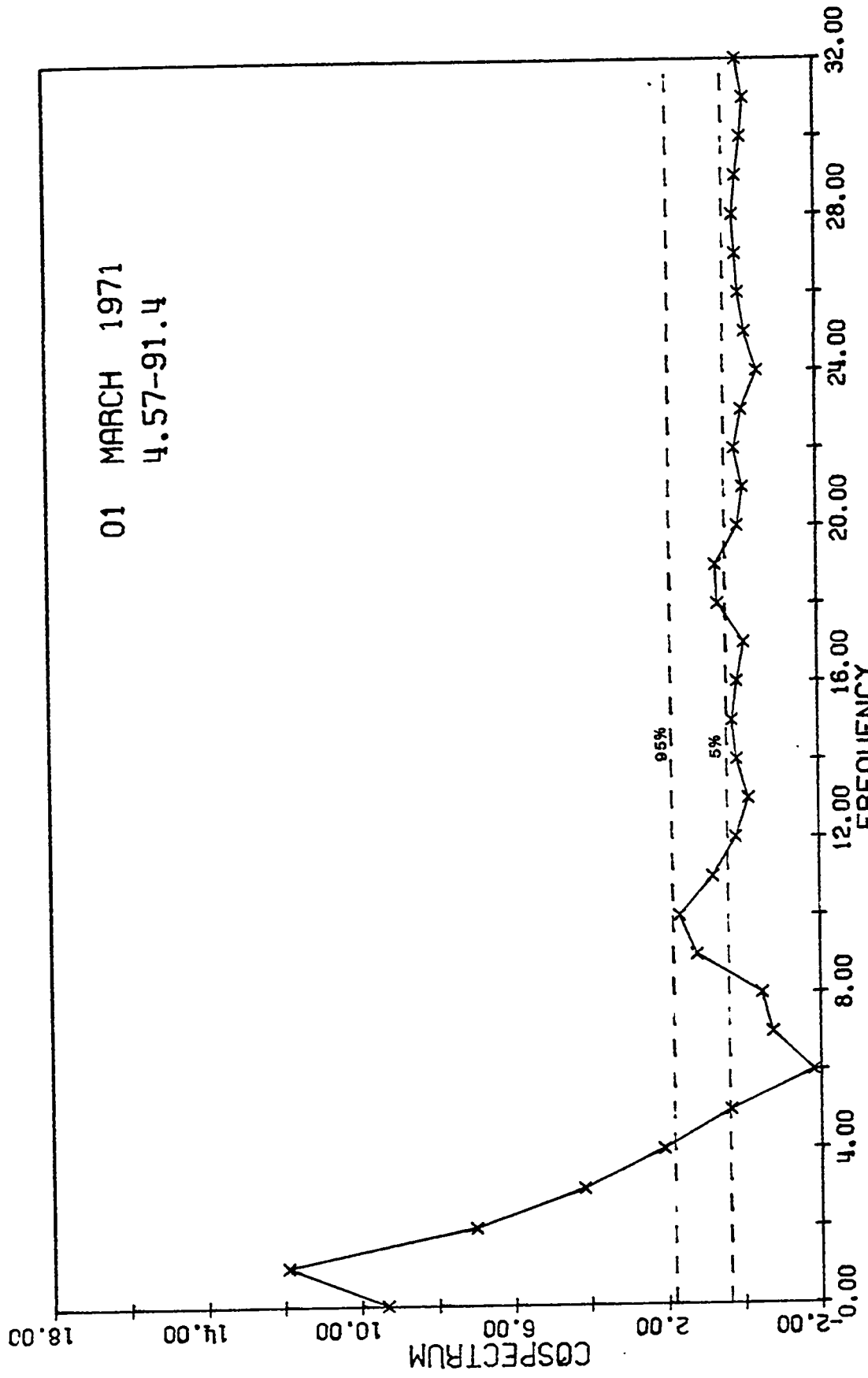

Figure A-12. Cospectrum of temperature. Normalized cospectrum versus frequency (cycles per 128 min.).

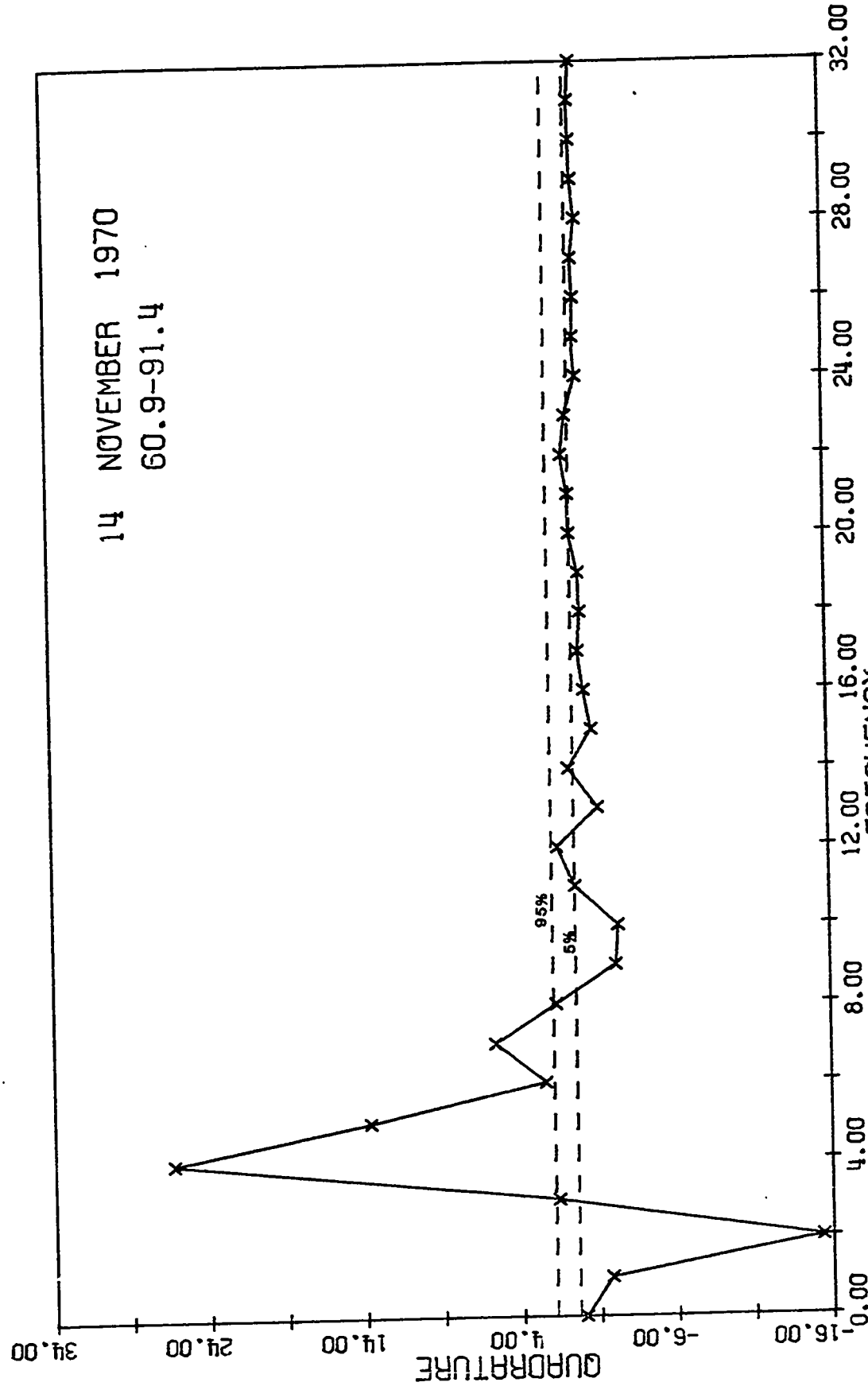

Figure A-13. Quadrature spectrum of temperature. Normalized quadrature spectrum versus frequency (cycles per 128 min.).

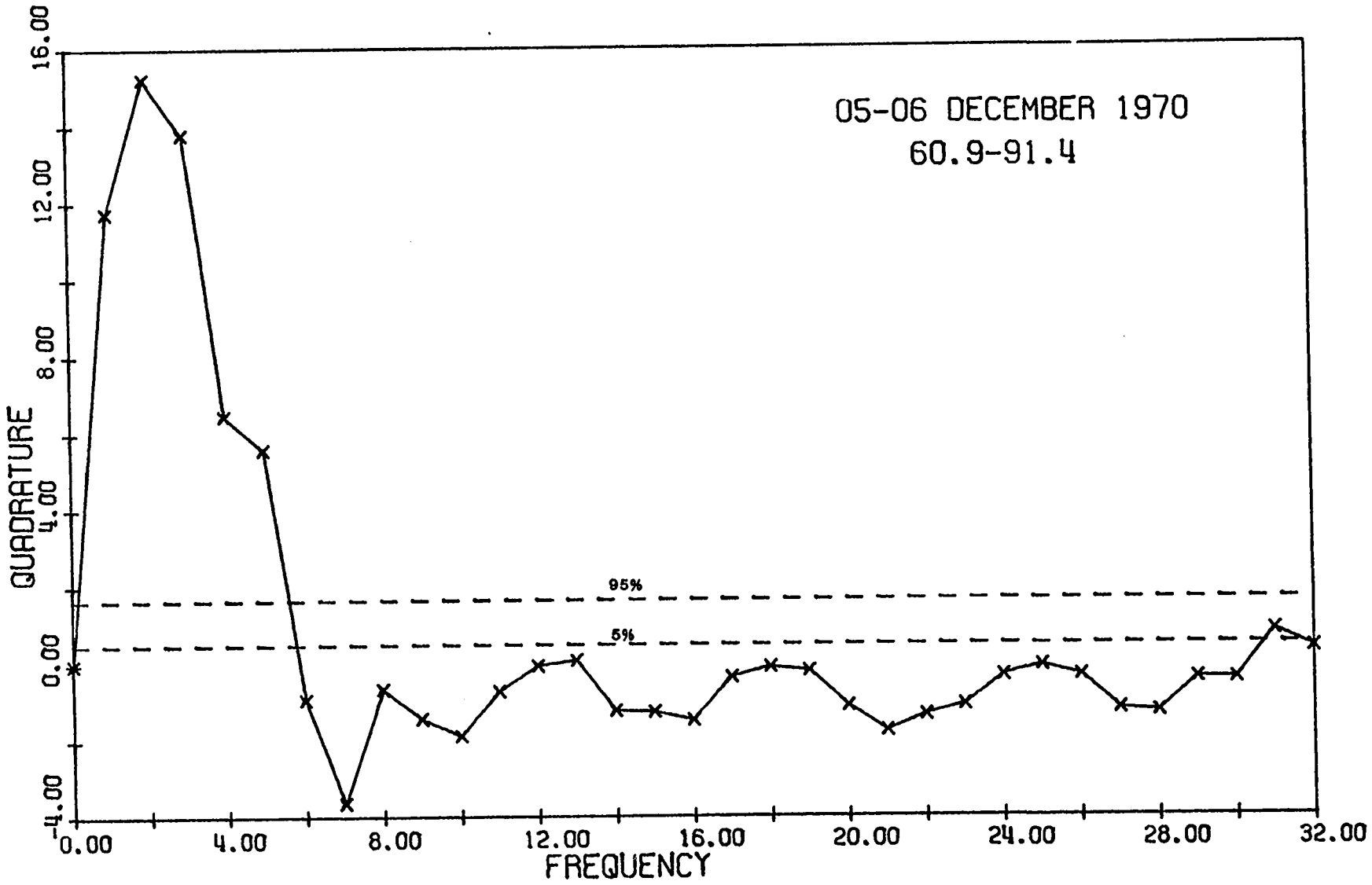

Figure A-14. Quadrature spectrum of temperature. Normalized quadrature spectrum versus frequency (cycles per 128 min.).

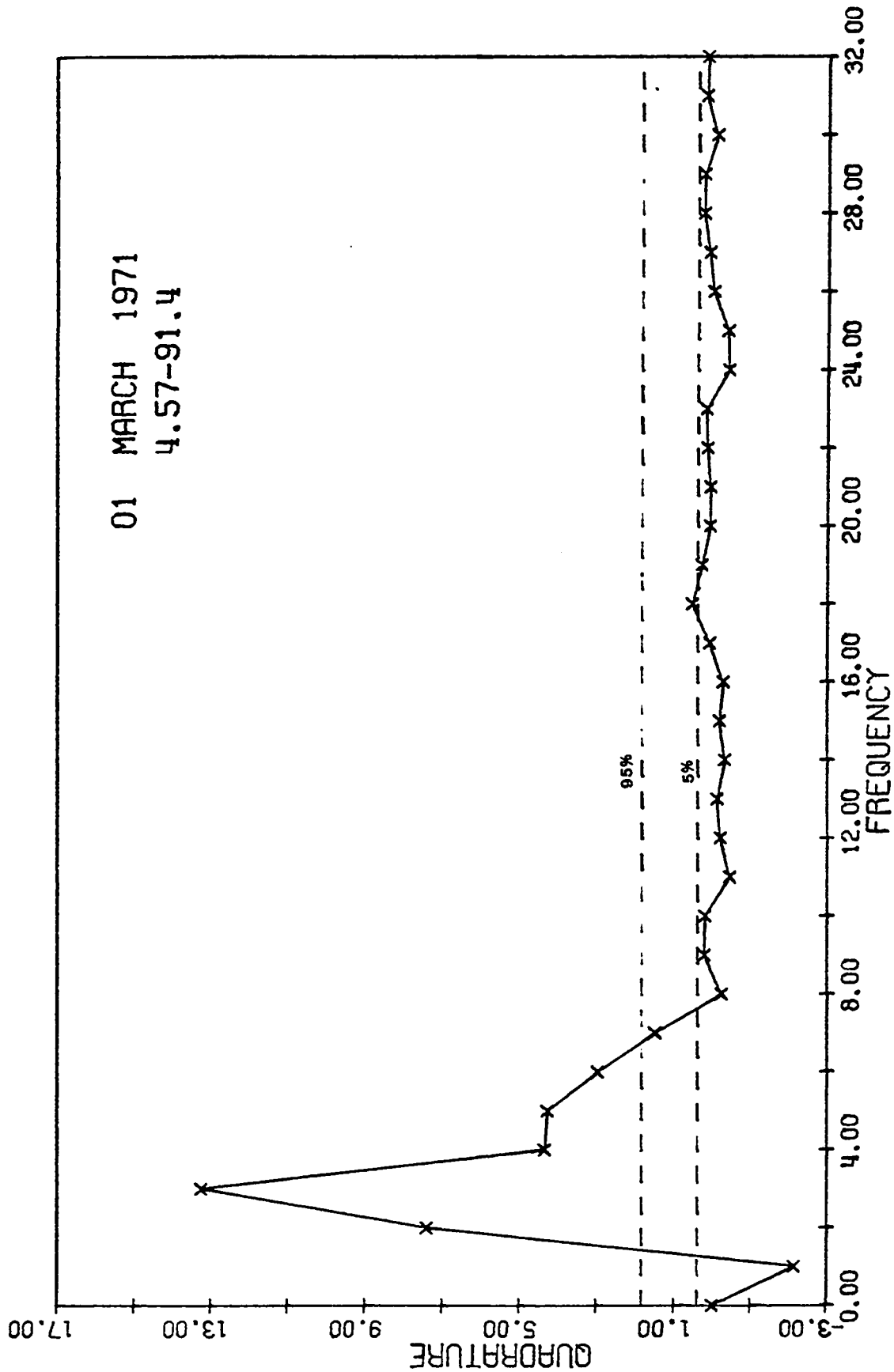

Figure A-15. Quadrature spectrum of temperature. Normalized quadrature spectrum versus frequency (cycles per 128 min.).

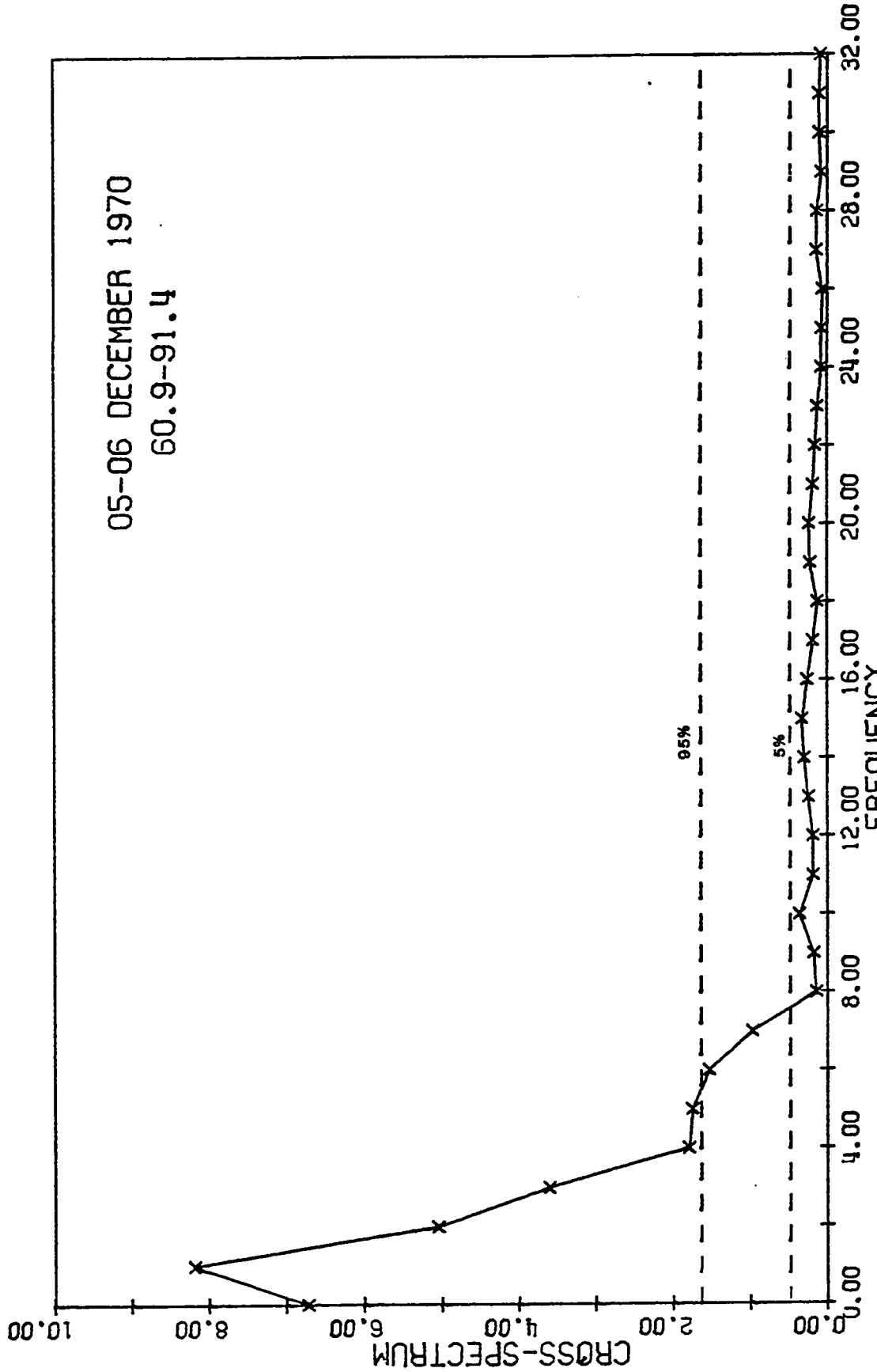

Figure A-16. Cross-spectrum of temperature. Normalized cross-spectrum versus frequency (cycles per 128 min.).

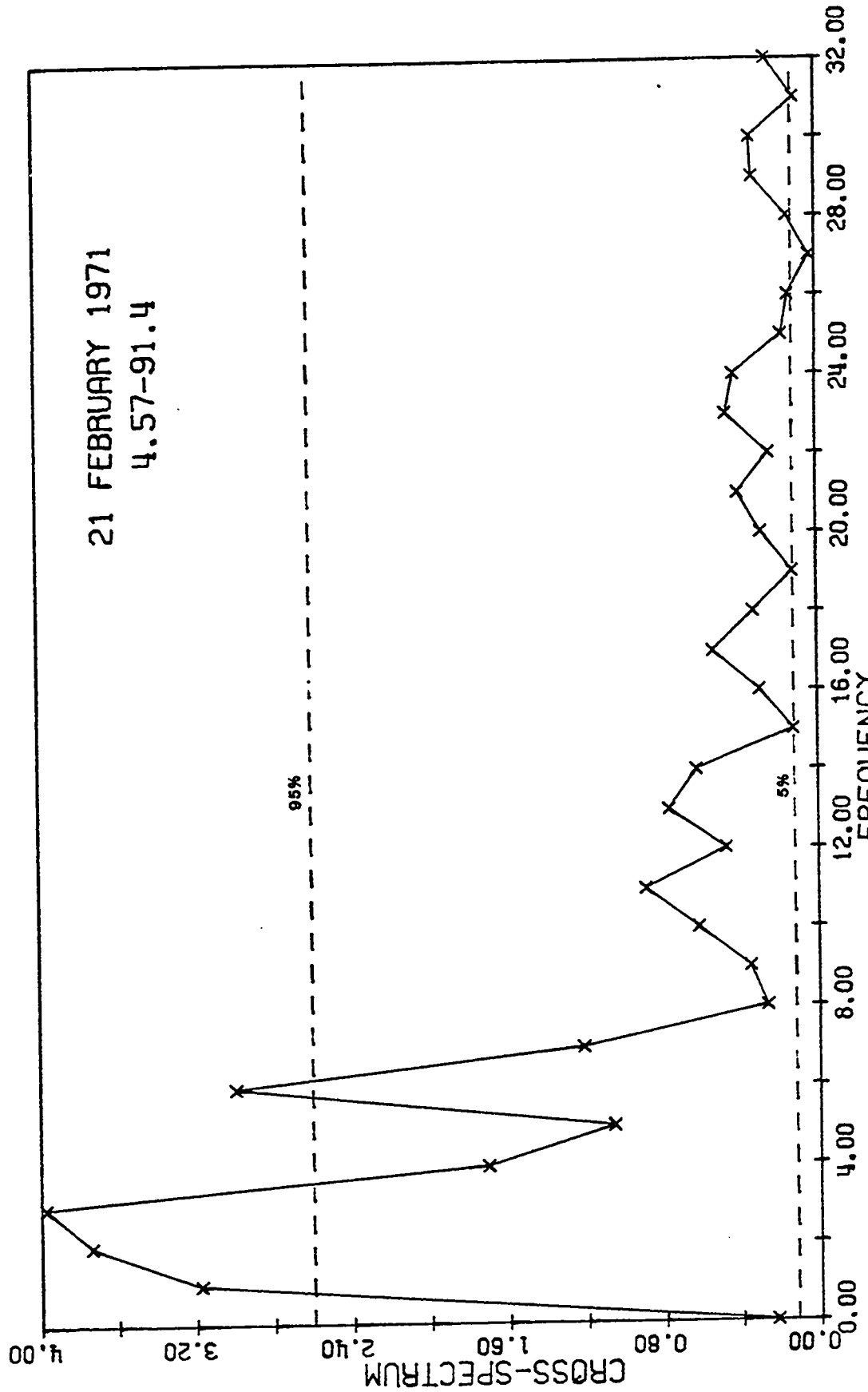

Figure A-17. Cross-spectrum of temperature. Normalized cross-spectrum versus frequency (cycles per 128 min.).

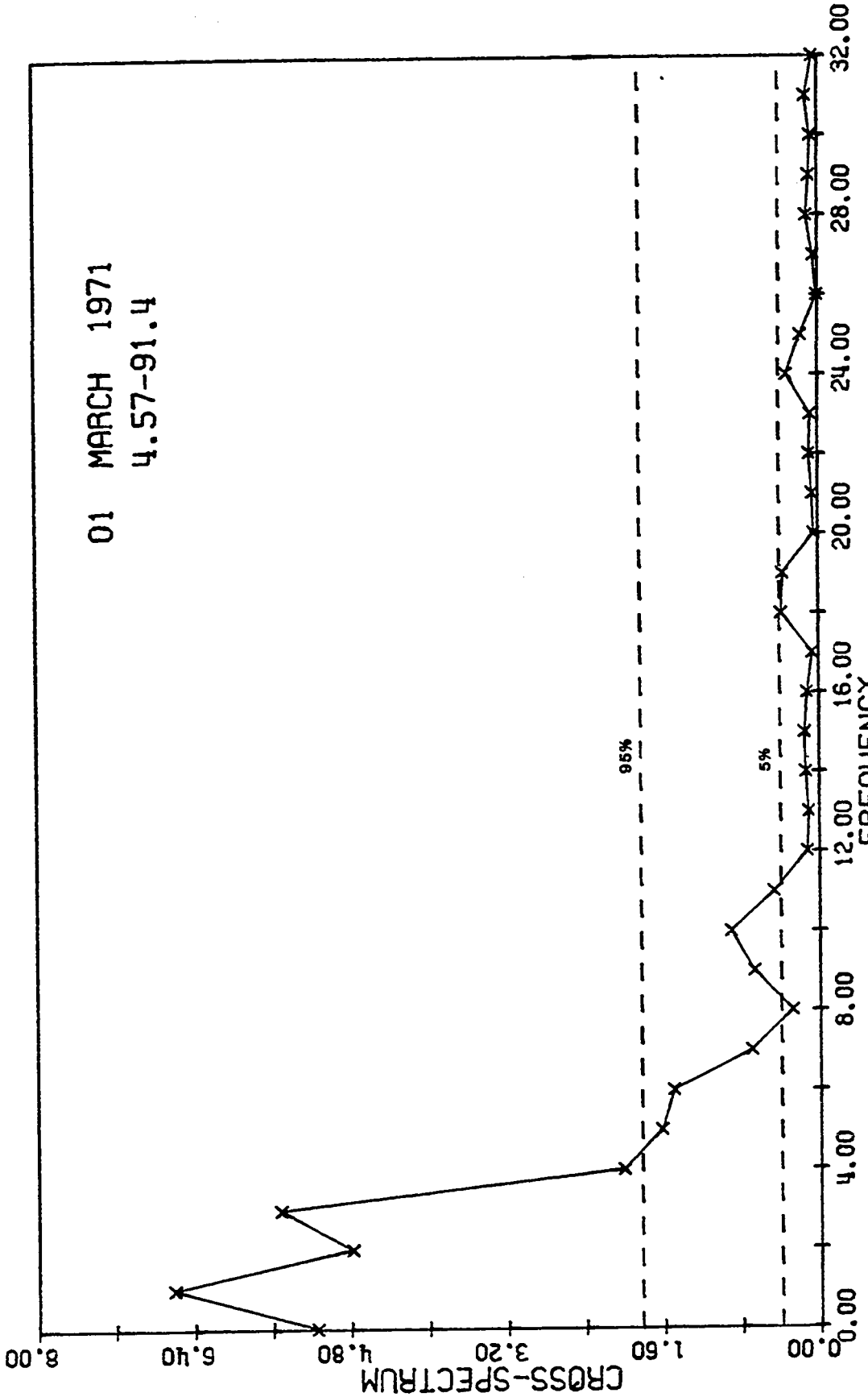

Figure A-18. Cross-spectrum of temperature. Normalized cross-spectrum versus frequency (cycles per 128 min.).